5-1-2019

A goal-oriented, inverse decision-based design method for designing football helmets

Tate Russell Fonville

A goal-oriented, inverse decision-based design method for designing football helmets

By

Tate Russell Fonville

A Thesis
Submitted to the Faculty of
Mississippi State University
in Partial Fulfillment of the Requirements
for the Degree of Master of Science
in Mechanical Engineering
in the Bagley College of Engineering

Mississippi State, Mississippi

May 2019

A goal-oriented, inverse decision-based design method for designing football helmets

By

Tate Russell Fonville

Approved:

_____

Mark F. Horstemeyer
(Major Professor)

_____

Youssef Hammi
(Committee Member)

_____

Farrokh Mistree
(Committee Member)

_____

Matthew W. Priddy
(Committee Member)

_____

Yucheng Liu
(Graduate Coordinator)

_____

Jason M. Keith
Dean
Bagley College of Engineering

Name: Tate Russell Fonville

Date of Degree: May 3, 2019

Institution: Mississippi State University

Major Field: Mechanical Engineering

Major Professor: Mark F. Horstemeyer

Title of Study: A goal-oriented, inverse decision-based design method for designing football helmets

Pages in Study 111

Candidate for Degree of Master of Science

We present a goal-oriented, inverse decision-based design method to find satisficing solutions for multiple football helmet components that all work together to achieve a set of conflicting goals. The efficacy of the method is illustrated with the design of the top region of an American football helmet. The prototype helmet was first constructed and tested with a twin-wire drop tower to study the different components effect on the system response. The inverse design method is used to design the foam liner to dissipate the maximum impact energy, and then the composite shell is designed to reduce the weight. The Concept Exploration Framework and the compromise Decision Support Problem are used to find satisficing solutions to the system-level performance goals under uncertainty. The proposed goal-oriented, inverse decision-based design method is generic and will be used to design additional components, the complete helmet, and ultimately helmets for other sports.

DEDICATION

I dedicate this work to God my heavenly Father. He is the author of all knowledge, the wind inside my sails, the light upon my path, my firm foundation, and the fire inside my veins.

ACKNOWLEDGMENTS

I want to acknowledge that my opportunity to earn a master's degree in mechanical engineering was only possible from the collective effort of my family, committee members, MSU faculty and staff, my colleagues, mentors, wife and God. I want to thank my mother and father for always supporting me, for offering wisdom during my challenging times, and their enduring love through it all. I especially want to thank my wife Chandler who is a constant source of love and support. Every day is new, and every day she goes above and beyond to support me and love me in many ways. I want to thank the Buntin and Todd family also, who showed me true family love and cared for me as their own. I want to acknowledge each of my committee members for their guidance, correction, and patience. Dr. Priddy for his advice and leadership, Dr. Youssef for always assisting with my challenges, and Farrokh for always going above and beyond to teach me and correct me with my work. I have learned a great deal from each of them and feel equipped now to pursue my PhD. I want to thank Dr. Mark especially for investing in me and having faith in me. I have grown a great deal personally, spiritually, and academically thanks to his sound wisdom, leadership, and advice. Finally, I want to acknowledge all the help from the MSU faculty and staff, my colleagues at CAVS, and my academic and spiritual mentors. I could not have made it through this degree without their help.

TABLE OF CONTENTS

LIST OF TABLES

LIST OF FIGURES

CHAPTER I

FOUNDATIONS FOR HELMET DESIGN

1.1 Introduction

In this thesis, we lay the foundation for football helmet design using a goal-oriented, inverse decision-based design method for multi-component product systems. First, we designed, built, and tested a prototype football helmet in a more traditional "trial-and-error" way to gain insight into the complexities of product systems design. Most engineers and designers are familiar with the traditional trial-and-error strategy that is broken into three phases, namely, the research and design phase, the manufacturing phase, and the testing and analysis phase. In many cases, the designer repeats this cycle until arriving at a satisfactory or optimal design. For many small-scale systems, this approach can be a powerful tool to learn about the prototype and discover critical flaws. Unfortunately, this method can also be unpredictable, time consuming, expensive, and full of engineering errors. For industrial applications, launch-dates and budget restrictions limit the number of design iterations, and thus limit the amount of information gained through additional iterations. Typically, the lack of information results in a design change after the launch-date, which may be very expensive.

On the other hand, using a method that employs simulation-based design may mitigate the effects of post-launch design changes. Here, the designer or engineer can model the prototype geometry with a Computer Aided Design (CAD) program, run

computer simulations, and then quickly iterate on design scenarios with a range of computational tools. The simulation-based design paradigm does not necessarily reduce the time, costs, or uncertainties during the conceptual design phase, but does allow the designer to repeat the process in a fraction of the time in the overall design process to gain more information about the product, leading to better decisions by the launch-date. The obvious trade-off in computational expenses comes with the fewer design changes needed late into the development process. Therefore, with respect to football helmet design, we require a design method that supports simulation-based design to allow us to cycle through many helmet design iterations to arrive at a satisfactory design before product launch.

In Section 1.2, we briefly discuss the motivation behind football helmet design including an overview of brain injury related research, football's concussion crisis, and the NFL's "Play Smart. Play Safe" initiative. Then, in Section 1.3, we review the helmet technology advancements made at Mississippi State University (MSU) that form the foundation for our prototype helmet. In Section 1.4, we describe the experimental investigation of our prototype helmet and discuss the limitations of the traditional trial-and-error method. We end Chapter 1 with requirements for a method to design helmets with simulation-based design while considering uncertainty. In Chapter 2, we introduce the goal-oriented, inverse decision-based design method we selected for helmet design. In Section 2.1, we introduce and review the design method including the key constructs, namely, the Concept Exploration Framework (CEF), the compromise Decision Support Problem (cDSP), and solution space exploration with ternary plots. We use the CEF to systematically collect and manage component information for design analysis. The cDSP

is the core mathematical construct we use to generate design alternatives and then we can explore the solution space and make decisions with ternary plots. We demonstrate the design method in two ways. In Section 2.2, we demonstrate the CEF and cDSP constructs to design a single helmet component, namely, the helmet liner. In Section 2.3, we demonstrate the full method to design two components, namely, the foam liner and composite shell together with respect to the same set of system-level goals. Finally, in Chapter 3, we discuss the limitations in our method and future work.

1.2 A Historical Overview of the Concussion Crisis in American Football

American football (at the professional and collegiate level) has been the most watched sport in the United States since 1985 [1]. While the sport itself is exciting to watch, in recent years mild traumatic brain injury (MTBI), also called concussions, and the neurodegenerative brain disease Chronic Traumatic Encephalopathy (CTE) have taken the spotlight. In the sport's early days, the game was rough with little to no equipment or rules available to protect the athletes from injury. That was until John T. Riddell founded the sports equipment company Riddell in 1929. Riddell critical helmet innovations through the 1900's addressed prevalent injuries such as cauliflower ears, broken facial bones, or skull fracture. In the 1930's they were the first to introduce the hard plastic shell, then chinstraps and helmet suspension systems in the 1940's, faceguards in the 50's and many more developments that make up the iconic football helmet we have today [2]. These developments were not engineering efforts, but rather a form of necessity-based innovation.

Head injury related research did not begin until the 1940's, and primarily focused on external effects, such as skull fracture. Researchers at Wayne State University [3]

dropped human cadavers onto steel slabs to study the effects of impact force and location to skull fracture and brain damage. Data collected from the human cadaver research led to the development of a foundational head injury metric in 1960, namely, the Wayne State Tolerance Curve (WSTC) [4]. We show the modified WSTC, including sub-concussive data from [5] in Figure 1.1 below. The curve shows the correlation between linear acceleration (g levels), duration of impact, and risk to human life. From the WSTC we see that g levels, or sustained durations, above the line would result in a loss of human life.

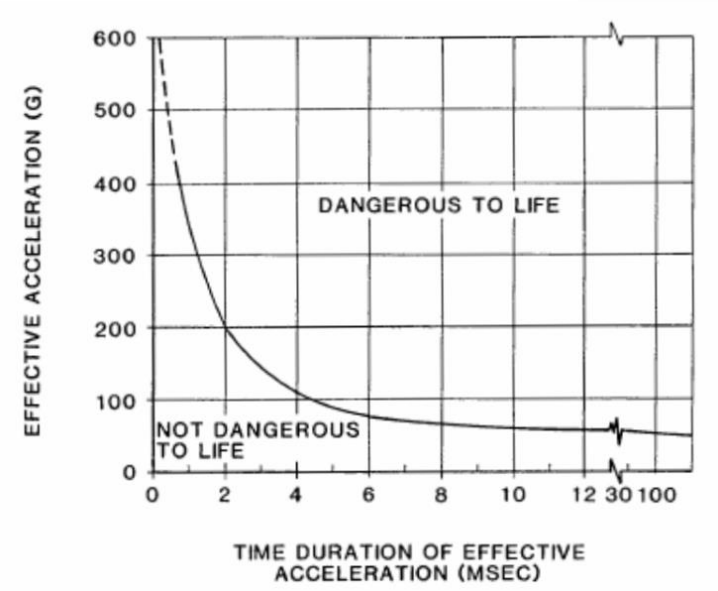

Figure 1.1 The Wayne State Tolerance Curve showing an early estimation of the effective acceleration vs. acceleration duration tolerance limit for the human brain [4].

Researchers at Wayne State developed the WSTC in response to the high number of fatalities and injuries in the automotive industry. The sports industry experienced a similar trend, with a high number of injuries each season and 32 fatalities in 1968 [6]. Helmet technology at the time was not sufficient to protect the players that led to the

establishment of a set of helmet safety standards through the National Operating Committee on Standards for Athletic Equipment (NOCSAE) in 1970. The first set of NOCSAE standards were inspired by automotive industry standards and used head injury metrics derived from the WSTC. The primary head injury metric used in all NOCSAE standards in the Gadd Severity Index, or simply the "Severity Index" (SI) [7]. The SI is based on the following equation,

$$SI = \int_0^t a(t)^{2.5} dt \tag{1.1}$$

were $a(t)$ is the resultant acceleration time history normalized by gravity (G's), t is the duration of the impact in seconds, and 2.5 is the power-weighting factor derived from the WSTC. The SI is measured during a NOCSAE standard twin-wire drop test [8] where a standard instrumented NOCSAE headform is dropped onto a test anvil from 2, 3, 4, and 5-foot heights. A standard NOCSAE headform is instrumented with a tri-axial accelerometer at the center of gravity that records linear acceleration. The resultant acceleration time history is used to calculate the SI. According to NOCSAE standards [8], no test should exceed a SI value of 300 at the lowest impact height, and no test should exceed a SI value of 1200 at the higher impact heights. While the SI is still used in NOCSAE standards today, Versace et al. [9] criticized the SI injury metric because it does not provide a distinction between the fitted WSTC data, severity scaling, and the magnitude of the acceleration pulse, or "effective acceleration". They proposed a variation of the SI that focuses only on the effective acceleration, known as the Head Injury Criterion (HIC). The HIC has its roots in the work of Gurdjian et al. [10-12] who developed head injury tolerance data from live animal and human cadaver experiments

and used the HIC functional to evaluate sports helmets. The HIC functional was formally derived by Hutchinson et al. [13] as,

$$HIC = [(t_2 - t_1)\{\frac{1}{(t_2-t_1)}\int_{t_1}^{t_2} a(t)dt\}^{2.5}] \quad (1.2)$$

where t_1 and t_2 represent the start and finish of the effective acceleration peak, $a(t)$ is the resultant acceleration time history, and 2.5 is the same power-weighting factor derived from the WSTC. The HIC injury metric is most commonly used in the certification of newly manufactured vehicles. Prasad et al. [14] used the HIC functional to develop a Head Injury Risk Curve (HIRC). According to the HIRC, 50% probability of life-threatening brain injury can result from a HIC value around 1400, where only 18% probability from a HIC value of 1000. In this thesis, we use both the SI and HIC injury metrics, along with the Peak-G, to assess the performance of an American football helmet prototype with our own twin-wire drop tower test system and the NOCSAE standard drop-test method. While the SI, HIC, and Peak-G injury metrics may be commonly used to certify and evaluate helmet performance, it is important to remember that these injury metrics and NOCSAE standards are approximations and can only predict the risk of skull fracture with respect to linear acceleration. They do not provide insight into the brains response or predict the risk of MTBI or CTE. To engineer better and safer football helmets, we must understand the biomechanics of the brain and develop injury metrics that can predict MTBI.

Several researchers have worked to understand the biomechanics of the brain under impact loading. Some of the foundational assumptions for brain related research were established by Holbourn et al. [15] in 1943. From their prospective, they assumed the brain material to be of uniform density, nearly incompressible but having a small

modulus of rigidity. Because of the brain's incredibly high bulk modulus (incompressibility) yet low modulus of rigidity, they predicted concussions were either a result of skull fracture or shear strain in the brain. Holbourn hypothesized that the translational accelerations from impact were non-injurious while the rotational accelerations caused the high resultant shear stress and consequently concussions. Using the Holbourn hypothesis as a foundation, many researchers have attempted to develop a concussive threshold with cadaver experiments, live animal testing, impact reproduction, FEA, and on-field observation with instrumented helmets. Ommaya et al. [16] performed human cadaver experiments to study the relation between acceleration and intracranial pressure. They found that an inverse correlation exists between acceleration and pressure, where a shorter acceleration duration would require higher pressures to result in concussion and vice versa. They also point out that any system that can increase the time duration of an impact in an equal or diminished ratio to the decrease in acceleration or pressure will result in a safer system with respect to MTBI. Ommaya et al. [17] went on to develop one of the first cerebral concussion tolerance curves with live animal impact testing. They were able to produce a tolerance curve for three primate species, and then extrapolated the data to include humans. Their curve suggests rotational accelerations greater than 1800 rad/s^2 would result in a concussion. Pellman et al. [18-19] was able to reconstruct 31 NFL game impacts, including 25 diagnosed concussions, using test dummies to study linear and rotational accelerations and develop a concussive threshold. They determined concussions were primarily related to linear accelerations in the 70-75g range and did not find any significant correlation between rotational accelerations and head injury. Zhang et al. [20-21] validated the Wayne State University brain injury model

(WSUBIM) and then used it to simulate head impacts to propose a new injury threshold for MTBI. The WSUBIM Finite Element (FE) head mesh contains 314,500 elements and 281,800 nodes, it can differentiate between white and grey matter, and contains anatomically detailed facial bones. Like Pellman et al. [18-19], they reconstructed 24 head impacts in their lab with test dummies and hybrid III instrumented headforms. Then, they applied the centroid acceleration data to the WSUBIM FE mesh to study different stresses in the middle of the brain. They found that shear stresses in the brain stem were highly correlated to rotational acceleration. They proposed a new 50% concussion probability tolerance limit for shear stress, translational (linear) acceleration, rotational acceleration, and HIC values of 7.8 kPa, 85 g, 6000 rad/s^2, and 240, respectively. Patton et al. [22] used a significantly smaller head mesh, consisting of only 11,158 elements, to recreate 27 concussive and 13 non-concussive impacts to develop a strain tolerance limit. They suggest a 50% concussive probability from upper strain limits of 0.13, 0.15, and 0.26 in the thalamus, corpus callosum, and white matter, respectively. While FEA may offer precious insight into the brain's response under impact loading without the risk of actual injury, there can still be a great deal of uncertainty in the mesh, material models, assumptions, and boundary conditions. Therefore, some researchers instrumented players helmets with the Head Impact Telemetry (HIT) system to capture helmet impact data from live practices and games. Funk et al. [23] studied 27000 head impacts with only 4 reported concussions to develop a concussion risk curve from unbiased data using the peak-g or HIC injury metrics. They compared their risk curve to the biased curves produced by Pellman [18-19] and Zhang [20-21] to reveal their false predictive capabilities. Funk finds a 10% MTBI risk from peak linear acceleration, angular

acceleration, and HIC values of 165 g, 9000 rad/s^2, and 400, respectively. After Funk et al. [23] revealed the predictive flaws of biased risk curves, many other researchers attempt to nail down the concussive threshold values using the HIT system. McCaffrey et al. [24] used the HIT system data to study the balance and neurocognitive function of participants who sustained a 90 g impact or higher. They found that non-concussed football players did not exhibit a decline in balance or cognition after exposure to an impact greater than 90 g. Broglio et al. [25-26] used the HIT system with high school players to study linear and rotational acceleration, jerk, force, impulse, and impact duration categorized by season type, player position, and helmet impact location. They were able to capture 13 concussions and proposed a threshold for linear and angular acceleration values of 96.1 g and 5582.3 rad/s^2 respectively. They also identified the top, front, and back locations having the highest probability for concussions. Rowson et al. [27-28] studied 76000 head impacts with the HIT system and a 6 Degree of Freedom (DOF) rotational acceleration sensor system to reproduce impacts with an FE model. They used the Cumulative Strain Damage Measure (CSDM) to find a strain threshold of 0.15. Rowson et al. [29] then studied 300,997 head impacts, including 57 concussions, with the HIT system and the 6 DOF rotational acceleration system to develop a concussion risk function for rotational head kinematics. They break down their results by injury risk from 10% to 90% and report values for rotational acceleration ranging from 5260 to 7483 rad/s^2 and rotational velocity ranging from 23.3 to 33.2 rad/s. To further substantiate the debate on a concussive risk tolerance curve, Duhaime et al. [30] used the HIT system to study 486,594 head impacts, including 48 concussions, but reported a spectrum of concussion-causing linear and rotational acceleration values ranging from

16.5 to 177.9 g and 183 to 7589 rad/s^2, respectively. This new data revealed the uncertainty associated with any universal predictive concussive threshold. Crisco et al. [31] found that player position and helmet impact location had a large influence on concussion. They determined the top of the helmet resulted in the largest peak linear accelerations and the front/back resulted in the largest rotational accelerations. They also identified the running back to have the highest linear acceleration, followed by the linebacker, and the defensive back. Finally, to consolidate the concussive risk prediction, Rowson and Duma [32] developed a new injury metric, the combined probability of concussion, from 63,011 impacts collected by the HITS system. The combined probability of concussion metric computes the overall risk of concussion based on both the peak linear and rotational accelerations and varies weights on sub-concussive or concussive level impacts and unreported or undiagnosed concussions. They find that the combined metric is far better at predicting concussion than either the linear or rotational metrics alone. While there may not be conclusive evidence leading to a specific injury threshold, the data collected by the NFL and the HIT system are still useful for helmet design. One of the largest studies reported in literature [33] uses the Head Impact Telemetry (HIT) system to collect data from 8 collegiate teams from 2005 to 2010, including 1833 players and a combined total of 1,281,444 head impacts. Through the course of the study, they track concussions for two Riddell helmets, the VSR4 and the next generation Revolution. They find that the helmet design update from the VSR4 to the Revolution resulted in 53.9% less concussions. While this observation is limited to only two helmet models, the simple fact that a helmet update can reduce the risk of concussion gives the current efforts to design a safer football helmet a positive outlook.

When concussions first became a major concern for football back in 1994, the NFL's MTBI committee regarded them simply as an "occupational risk." It was not until 2002, when Dr. Bennet Omalu made the discovery of CTE in Mike Webster's brain [34] and then linking it to repeat MTBI sustained during his football career that the NFL's MTBI committee began taking the link between football and brain injury seriously. Dr. Omalu continued to link CTE to football with multiple confirmed CTE diagnosis in deceased football players. In 2010, the NFL began funding Dr. Ann McKee's team at Boston University to research factors that contribute to CTE. Dr. McKee's group's primary contributions include linking CTE to sub-concussive impacts [35], and a study [36] that found CTE in 177 of the 202 brains of football players.

The Boston University Research CTE Center [37] defines CTE as a "progressive degenerative disease of the brain found in people with a history of repetitive brain trauma, including symptomatic concussions as well as asymptomatic subconcussive hits to the head that do not cause symptoms." From what we know today, CTE is the result of a buildup of an abnormal protein called tau that is responsible for brain degeneration. Common symptoms of CTE may include memory loss, aggression, depression, dementia, and others that all may become develop after repetitive concussions or a long while later. As it stands, the only way to diagnose CTE is through brain dissection postmortem, but McKee et al. [38] found it develops in the four stages, shown in Figure 1.2 below.

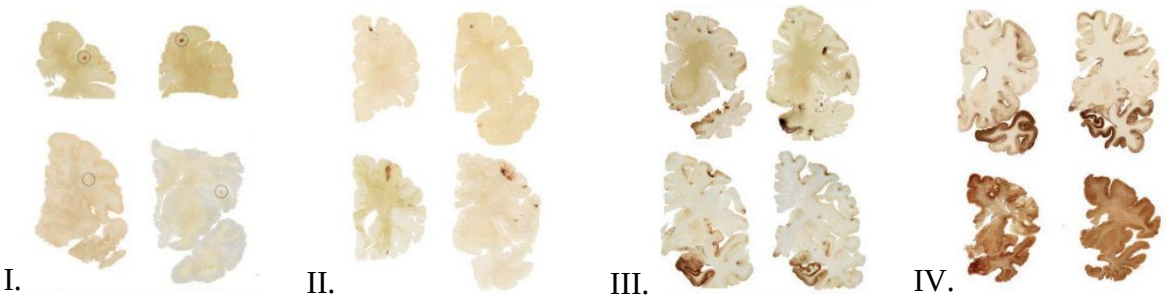

Figure 1.2 The four stages of CTE [38]. I-Tau protein is identified in the cerebral cortex as small brown spots. II-The progression of the tau as it spreads to adjacent cortices. III-Widespread CTE to the frontal, insular, temporal and parietal cortices. IV-Severe tau protein affecting most of the cerebral cortex and medial temporal lobe.

Mounting concerns over MTBI and CTE met a climax in 2011 when 4,500 former athletes sued the NFL for $765 million to settle damages for over 18,000 athletes caused by the league's misinformation, research, and denial [39]. In the lawsuit aftermath, the NFL began to turn things around by launching the "Play Smart. Play Safe" initiative through their startup nonprofit organization, Football Research, Inc. The "Play Smart. Play Safe" initiative is focused on four primary areas: protecting players, advancing helmet technology, funding medical research, and sharing progress. Some of their primary contributions to-date include implementing rule changes, establishing concussion protocols, funding neuroscience/concussion research, hosting youth concussion awareness programs, and funding towards helmet technology innovations. Their engineering roadmap provides funding for a series of Head Health Tech Challenges (HHTC) that support research and development directly related to improving player protective equipment [40]. The focus of this thesis is on the prototype helmet developed in conjunction with Yobel Technologies LLC. for submission to the HHTC program. In the next section, we give an overview of the components that make up our prototype football helmet.

1.3 Football Helmet Technology to Protect the Brain

The prototype helmet system comprises six components including a titanium faceguard, a rubber gasket, a polypropylene (PP) with short E-glass fiber composite outer shell, a 3D printed nylon inner shell with bio-inspired sutures, 3D printed nylon stress-wave dampers, and a foam liner. We display the prototype helmet below in Figure 1.3

Figure 1.3 Our prototype football helmet showing the exploded view (left) and front view (right).

We believe a football helmet should have three key functionalities, to dissipate impact energy, trap momentum, and mitigate stress waves. Our goal is to design each component shown in Figure 1.3 above to work together to achieve these key functionalities. Johnson et al. [41] at Mississippi State University (MSU) came up with the design our first prototype faceguard. They took inspiration from big-horn sheep impact research and hypothesized that the topology of the faceguard could be optimized to reduce tensile pressure and shear strain in the brain. They created a finite element analysis (FEA) of a NOCSAE standard linear impactor test that strikes the faceguard at 6 m/s in two common locations “A and A’” determined by [18-19, 42-43]. They modeled

the facemask as titanium (Ti-6Al-4V) with elastic properties and set a hard design constraint against plastic deformation. They used a full-scale human head mesh created from Computed Tomography (CT) scans that comprises skin, cortical bone, cancellous bone, cerebral spinal fluid (CSF) and brain. They modeled the brain behavior with the MSU TP 1.1 an Internal State Variable (ISV) [44-45] and then validated it with human cadaver experiments [46]. They created a surrogate model from ten Design of Experiments (DOE) points to replace the computationally expensive full-scale FEA. Finally, they found optimal designs using a Nondominated Sorting Genetic Algorithm (NSGA-II) [47] with constraints on solid fraction and bar geometry. The optimal design was able to reduce tensile pressure in the brain by 7.5% and maximum shear strain by 39.5%. We recreated the optimal faceguard geometry in SolidWorks (Dassault Systems, Waltham, MA) and verified the dimensions with Johnson's original CT scan. We show the faceguard SolidWorks model and cast geometry below in Figure 1.4.

Figure 1.4 Johnson et al. [41] optimized faceguard SolidWorks model (left) and titanium cast (right).

We modeled the faceguard grid curvature to match that of a standard football helmet faceguard. We positioned the vertical bars according to Johnson's [41] results. We then cast the design out of titanium (Ti-6Al-4V) and pressure treated it with Hot Isostatic Pressing (HIP) to reduce the porosity. Finally, we created CT scans of the cast faceguard to verify the microstructure after casting and treatment was acceptable. We designed the faceguard to mount flush with the composite shell to reduce the risk of another helmet grabbing any external hardware resulting in harmful torque on the neck. However, we place a soft rubber (Sorbothane) gasket between the faceguard and the shell to ensure a secure fit.

We selected two foam liner options for consideration. Rush et al. [48] optimized our primary foam liner design from a series of physical experiments with a standard NOCSAE twin-wire drop tower system. They selected slow recovery, open-cell viscoelastic polyurethane foam as the base foam material for optimization because of its excellent energy dissipation properties. Open-cell slow-recovery foams are similar to closed-cell foams, but allow for deformation. The cell walls have small holes that allow air to escape and return. This process is referred to as viscous dissipation and is the primary energy dissipation mechanism. The features that affect viscous dissipation include cell size, cell orientation, number of holes, and hole spacing on a cell wall. Under mechanical compression, the stress-strain behavior of an open-cell foam can be broken up into the three regions as shown below in Figure 1.5.

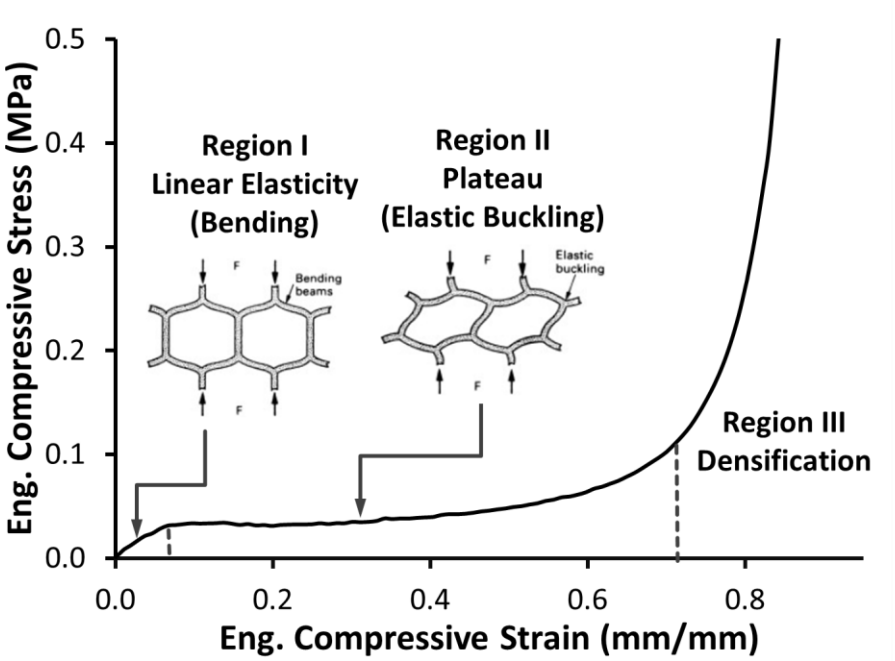

Figure 1.5 Three regions of compressive stress-strain behavior of open cell foams.

In Region I, the material behaves linear elastically, that is up until about 5% compression. A plateau (Region II) follows the linear elastic region where the material absorbs energy at a constant stress until about 60% compression. It is during the plateau region ($0.05 \leq \varepsilon \leq 0.6$), viscous dissipation occurs and most of the air within the cell structure escapes to the environment. Rapid densification (Region III) occurs from 60% compression up to about 80% compression when the empty cells collapse on each other.

Rush et al. [48] conducted a series of compression tests with various foam densities (87.0, 79.9, 82.8, 84.3, 85.6 kg/m^3) at lower strain rates (0.001, 0.01, and 0.1/s) and at high strain rates (600 and 1200/s). They found that the stress levels of the linear elastic, plateau, and densification regions all rise while the densification strain lowers with increasing strain rates. They also claim that increasing the foam density can achieve the same results.

They constructed a foam liner for a football helmet using the baseline foam and conducted a series of tests with the NOCSAE twin-wire drop tower system to learn how the foam enhances helmet performance. They found that the liner distributes the impact forces across the entire surface of the head that reduces localized stresses, the plateau-stress determines how much acceleration is transmitted to the brain, and the key to minimizing acceleration and average impulsive forces is to allow the foam to compress up to the rapid densification region. They identify that an optimal foam for helmet applications can be determined using peak acceleration (G's), rebound velocity, maximum strain, and strain energy as optimization metrics. Keeping these metrics in mind, they went on to find an optimal foam liner design using the NOCSAE twin-wire drop tower and a set of 12 experiments from an L12 Taguchi Array DOE. Each foam liner alternative was an array of cylindrical pods wrapped in Thermoplastic Polyurethane (TPU). In their experimental investigations, they considered gas, foam density, layers of density, dampers, foam length, Area Ratio (AR), pod diameter, impact location, and TPU thickness as design parameters. Where the gas is the medium inside each foam cell, the densities used were SunMate (Dynamic Systems Inc.) brand Medium (79.9 kg/m^3), Firm (84.3 kg/m^3), and Extra-Firm (85.6 kg/m^3), and AR refers to the ratio of foam to head surface area (from 0.5 to 1.0). They discovered foam pod length was the most important parameter followed by AR, foam density, and TPU wrap thickness. The optimal foam pod liner design consists entirely of 50.8 mm (1.5 inches) long cylindrical Firm foam pods (84.5 kg/m^3) with a TPU wrap thickness of 0.635 mm (25 mil) and an Area Ratio of 0.75. They tested their optimal foam liner design and compared the SI, HIC, and Peak-G

results with several commercially available football helmets to find their optimal liner significantly lowered all three results.

We used the same brand of SunMate (Dynamic Systems Inc.) polyurethane open-cell viscoelastic foam with our second prototype, but functionally graded the densities from Medium (79.9 kg/m^3) to Extra-Firm (85.6 kg/m^3) in layers through the cross section. Our hypothesis was if lower foam densities are more suitable for lower stress levels, and higher foam densities are more suitable for higher stress levels, then functionally grading layers of different densities will result in a liner that can dissipate energy at a range of impact levels. We show the Rush et al. [49] optimal foam pod liner and the prototype functionally graded foam liner cross section in Figure 1.6 below.

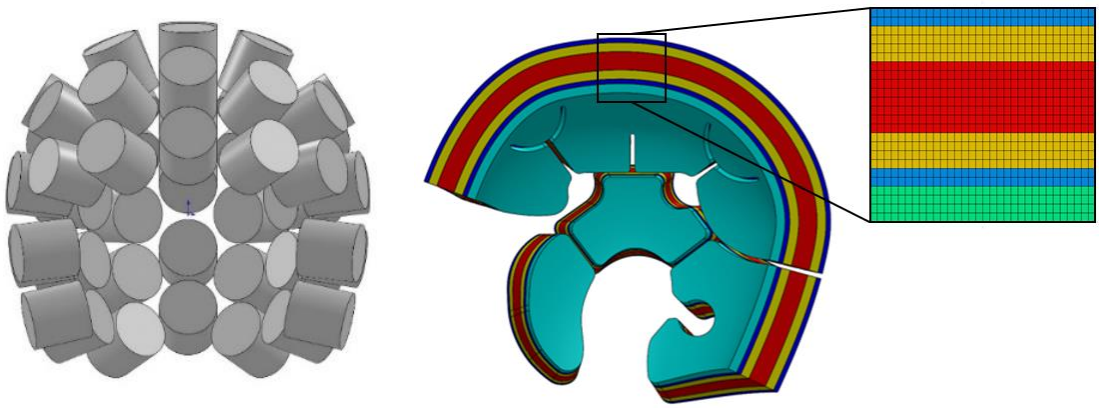

Figure 1.6 Rush et al. [48] optimized foam pod liner (left) and the prototype functionally graded foam liner (right). The functionally graded liner consists of four densities: Medium (79.9 kg/m^3), Firm (84.3 kg/m^3), Extra-Firm (85.6 kg/m^3), and Soft (87.0 kg/m^3) shown as blue, yellow, red and light green, respectively.

From preliminary 2D finite element calculations, we determined the best functionally graded foam liner design consists of five layers linearly graded in density foam from Medium (79.9 kg/m^3) as the outer layer, to Firm (84.3 kg/m^3), and then to Extra-Firm (85.6 kg/m^3) in the middle, then back down to Medium. Our prototype design

also includes a sixth layer of 12.7 mm (1/2 inch) thick Soft foam (87.0 kg/m^3) to provide a good fit to a player's head. In Figure 1.6 above, the Medium, Firm, Extra-Firm, and Soft layers are represented by the blue, yellow, red, and light green colors, respectively. We made the prototype functionally graded foam liner design to cover as much of the player's head as possible to protect against impact from any direction. We partition the liner into various regions with relief cuts to make manufacturing possible. We also provide spaces for ventilation and stress wave damper placement.

The composite outer shell, the bio-inspired inner shell, and the stress-wave dampers are all conceptual components. We selected a polypropylene with short E-glass (PP+E-glass) fiber injection-moldable composite made by RTP Company (Winona, MN) as the outer shell material. The available RTP Co. brand PP+E-glass fiber composites range in fiber density from 10% to 50%. Table 1.1 below shows the range of material properties available compared to a baseline polypropylene shell material.

Table 1.1 RTP Co. brand polypropylene with E-glass (PP+E-glass) fiber density, tensile strength, and tensile modulus for 10% to 50% glass fiber additive.

	Density (kg/m^3)	Tensile Strength (MPa)	Tensile Modulus (MPa)
Polypropylene	910	32	1724
10% E-glass fiber	970	46	3103
15% E-glass fiber	1000	54	3448
20% E-glass fiber	1030	60	4482
30% E-glass fiber	1120	76	6206
40% E-glass fiber	1210	90	8964
50% E-glass fiber	1330	97	11722

We selected the 30% E-glass option for testing as a compromise between stiffness and weight. We want the shell to be as still as possible to minimize the impact duration, which would effectively lower the net impulse. The inner-shell and stress wave dampers are both bio-inspired designs. The prototype inner-shell with sutures was 3D printed out of nylon. To reproduce the sutures, we first split the inner-shell into 8 regions, similar to the way a skull is broken up. We propagated a sine wave with varying amplitudes along the region boundaries and randomly selected amplitude peaks to create a mock suture. We believe the inner-shell will provide additional rigidity and the sutures may function to mitigate stress waves at their juncture. The stress wave dampers are also bio-inspired designs. Trim et al. [49] and Johnson et al. [50] noticed the high toughness and energy absorbent nature of bighorn sheep horns and their ability to protect the brain from injury. They hypothesized the taper and spiral geometry played a key role in mitigating the stress waves. They went on to perform a set of finite element simulations with four geometries to study the geometric effects on stress wave propagation [51]. They found that a tapered spiral geometry was able to reduce an impulse (measured as the integral of the pressure history multiplied by the cross-sectional area over the simulation duration) by an average of 98.3% regardless of the loading type or material studied. We see tapered spiral geometries in other animals such as the woodpecker who undergo high cycles of high energy head impacts with seemingly no damage to the brain. Lee et al. [52] studied the effect of the hyoid bone's curvature, taper, and bifurcations had on the stress wave propagation. They reached a similar conclusion and found that the hyoid bone curvature and taper, along with the surrounding muscle, was able to decrease pressure by 75% and dissipate 84% of the impulse. In response to these findings, we created a prototype stress

wave damper with a curved and tapered geometry to adhere directly to the inner-shell. We show the bio-inspired inner shell and stress wave dampers below in Figure 1.7.

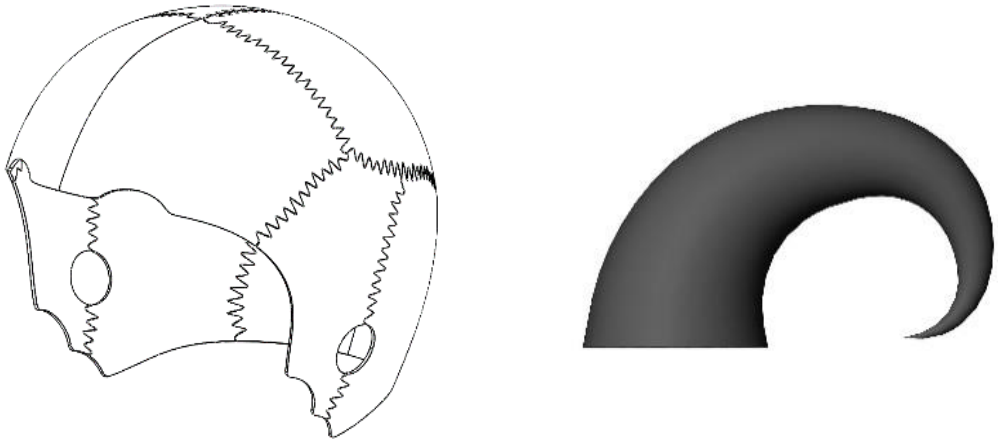

Figure 1.7 The bio-inspired prototype inner-shell with sutures (left) and stress wave damper (right).

There was some safety concerns about the damper geometry being curved and pointed. Therefore, we designed the structure to curve to a point where the point was directed away from the head, close to the base of the shell. We modeled the curvature using the golden ratio, which we commonly find in nature. In the next section, we discuss our experimental investigations with these prototype components to study their effect on each other as well as the overall system performance.

1.4 Helmet Experimentation With a Twin-Wire Drop Tower

In this section, we describe the twin-wire drop tower experiments conducted to understand the effect various helmet concepts had on each other as well as on the overall system response. We performed all drop tests with a NOCSAE standard twin-wire drop tower system, a standard 50th percentile adult headform, and a tri-axial accelerometer imbedded at the headform center of gravity (CG). We did not create or follow a DOE, but

rather the more traditional trial-and-error approach discussed earlier. Essentially, we formulated a hypothesis, configured the prototype helmet according to our hypothesis, conducted the drop test, made our observations, and then repeated the cycle. We dropped each helmet configuration in the top location, at 3ft. and 4 ft. heights, and recorded three common injury metrics, namely, the SI, HIC, and Peak-G.

We conducted tests with 11 different helmet configurations. While the results are interesting, only five stood out for discussion. In the first test, we compared a thin shell (≈2 mm) vs. a thicker shell (≈3 mm). In the second test, we compared the thin shell by itself to a thin shell with the bio-inspired inner shell with sutures. In the third test, we added the stress wave dampers to the inner-shell. In the fourth test, we removed the inner-shell and compared the performance of the stress-wave dampers directly adhered to the thin shell against the thin shell by itself. In the first four tests, we used the functionally graded foam liner where in the fifth test we compared the difference between the functionally graded foam liner to the optimized Firm foam pod liner.

In the first test, we found that the thin shell performed better than the thick causing the SI, HIC, and Peak-G values to drop by 8.5% on average. In the second test, we found that adding the inner-shell with sutures to the thin shell resulted in a loss in performance where the SI, HIC, and Peak-G values all rose about 11.6% on average. In the third test, adding the ram horns to the inner-shell caused values to rise by another 6%. After removing the inner-shell and adhering the stress wave dampers directly to the shell, we saw another rise in values by about 4.3% on average. Finally, when we compared the difference in the functionally graded liner to the Firm foam pod liner, we saw a drastic improvement in performance where the SI and HIC values dropped by approximately

30% and the Peak-G values dropped almost 12% on average. From our initial hypothesis, we expected the addition of the bio-inspired prototypes to improve performance, and the functionally graded liner to provide better protection than the Firm foam pod liner. The results from each of these studies showed the highly unpredictable nature of systems design. To understand the helmet system we would need to conduct more tests, however, due to time and financial restrictions we were limited to the number of design iterations we could perform. In the next section, we discuss how these observations led to the selection of the goal-oriented, inverse decision-based design method.

1.5 Selecting a Method for Helmet Design

In the previous section, we briefly described some of our experimental investigations with our prototype helmet system. We observed that the traditional design, build, test design cycle for multi-component product design is somewhat unpredictable, time consuming, and expensive. Simply combining optimal or ideal components together in the same system did not result in a predictable, or ideal system. Moreover, we would need many more design iterations to isolate an individual component's effects on the other components, or on the overall system. In addition, there is uncertainty in various forms and sources at every stage of the design, manufacturing, and testing process. Therefore, in order to design the assorted components of a football helmet together as a system we shift our paradigm from the traditional trial-and-error design paradigm to a new paradigm for decision-based system design.

In our new paradigm, we need to select a design method that supports simulation-based design, allows us to establish system-level performance targets and then design multiple sub-system components with respect to each other and the overall system-level

performance targets. The ideal design method should also support decision-making under the unpredictable uncertainty in the environment (aleatory), the predictable uncertainty in the design variables (epistemic), and the uncertainty associated with the modeling and analysis. The preferred design method must also be modular to allow for rapid sub-system component changes and design cycle iterations. Finally, we desire the method to be generic to allow us to design helmets for other sports in the future, such as hockey, lacrosse, or baseball.

We select the goal-oriented, inverse decision-based design method developed by the Systems Realization Laboratory @ the University of Oklahoma (SRL@OU) to design our helmet system. According to their decision-based design paradigm, systems design is the top-down driven, simulation-supported, inverse, decision-based design exploration of sub-system components that share the same set of system-level goals [53]. In decision-based design, the fundamental role of a human designer is to make decisions given that true optimality may be impossible because all models embody various forms of uncertainty [54]. Nellippallil et al. [55] originally demonstrated the efficacy of the goal-oriented, inverse decision-based design method for multiscale material and process chain design. In this thesis, we adopt their method and demonstrate its applicability to product design by designing two components of our conceptual helmet system. In Chapter 2, we discuss the details of the selected method and demonstrate its application to helmet design. In Chapter 3, we discuss our limitations and future work.

CHAPTER II

DEMONSTRATION OF THE GOAL-ORIENTED, INVERSE DECISION-BASED DESIGN METHOD FOR DESIGNING FOOTBALL HELMETS

2.1 A Goal-Oriented, Inverse Decision-Based Design Method Overview

In the previous chapter, we discussed our earlier attempts to design a prototype football helmet, comprised of six components ranging from conceptual to optimal, with a more traditional trial-and-error method. To recap, we list some of the **challenges associated with multi-component systems design** are listed below:

- System-level performance goals are seemingly unpredictable or unobtainable due to the complex interactions of multiple conceptual components within the same system boundary.
- Uncertainty is accumulated in three distinct ways: from the approximations in the math, material or analysis models used in the design phase, manufacturing quality control, and data collection or engineering errors in the experimental phase.
- Multiple iterations of the design, manufacturing, and experimentation phases required to gather enough information about the system to make good design decisions is highly time consuming.
- Analysis programs, computational resources, manufacturing and acquisition of materials, and test equipment can all be very expensive.

We view a football helmet simply as a "multi-component system" where at least two or more components, each with unique objectives, constraints, and variables, operate together within the same system boundary. To address the systems design challenges to design a football helmet, we require a design method that supports the following features:

- Supports decision-making in the presence of uncertainty
- Allows a designer to identify and manage complexity to account for the emergent properties that cannot be predicted
- Supports solution space exploration to find a compromise between satisficing solutions and costly iterations
- Supports simulation-based design
- Allows a designer to target system-level performance goals and then design multiple components with respect to those goals
- A modular and generic method to allow us to reformulate the problem at will and then substitute components to design for other helmets in the same product family.

To meet these requirements and find satisficing solutions for our helmet, we select the goal-oriented, inverse decision-based design method developed by Nellippallil et al. [56] for material and process design and adapt it for product design. The method is **goal-oriented** because we first select system-level performance requirements. This aspect of our method is inspired by Gero [57], who describes the Analysis, Synthesis, and Evaluation (ASE) design method as a series of information transformation beginning with an establishment of design requirements and ending with design specifications that satisfy the requirements. Gero's method [57] has five key aspects: functions, structures,

expected behavior, achieved behavior, and product descriptions. He defines a function as the relation between the design goal and the resultant behavior. A function can be formulated in terms of material, energy and signal (information). Structure represents the product subassemblies and their relationships identified during the analysis and synthesis phases. Structure contains information about the product geometry, materials, configurations, etc. The expected behavior represents the ideal, satisfactory product behavior and the achieved behavior is actual result. Finally, product descriptions are the structure specifications. Gero's method [57] for product design begins with establishing the system-level performance requirements. With respect to helmet design, these performance-requirements may include energy absorption or system weight requirements. In the analysis phase, functions are developed that describe the design requirements or goals to the product behavior in material, energy, or information terms. Then, product structure, expected behavior, and actual behavior can be generated through iterative synthesis and evaluation. Finally, product descriptions are found after the actual behavior satisfy the defined system-level performance requirements. The way Gero's method encompasses the ASE paradigm and maps product requirements to achieved behavior to find product description is useful in the development of our **goal-oriented**, inverse design method for designing helmets.

Our method is **inverse** because we design the individual components in an inverse manner with respect to the goals considering an initial forward mapping from a set of design requirements to design descriptions. The idea of forward mapping comes from Suh's Axiomatic Design Process [58]. Essentially, there are four key mapping sequences between four key domains to bridge "what we want to achieve" and "how we want to

achieve it." In the Customer Domain, Customer Attributes (CA) are the customer needs. In the Functional Domain, Functional Requirements (FR) are "what we want to achieve". In the Physical Domain, we identify Design Parameters (DP) that satisfy the FRs. Finally, in the Process Domain, we find Process Variables (PV) from the DPs. Suh's Axiomatic Design process requires effective mapping from the CAs, to the FRs, to the DPs, and finally to the PVs. There are two key axioms to Suh's design process:

- The "Independence Axiom" – where Design Parameters are mapped to the appropriate Functional Requirements such that modifying one Design Parameter will not affect other Functional Requirements.
- The "Information Axiom" – where any independent axiom has minimum information content.

According to Suh's Axioms, a good design is one that satisfies both Axioms. Regardless, the mapping between domains to achieve product requirements is useful for developing a method for decision-based design.

We support decision-making under uncertainty by incorporating aspects from Mistree et al. [59-61] Decision-Based Design (DBD) paradigm. According to their paradigm, the principal role of a human designer is to make decisions based on the information (decision support) provided by the computer. The designer should focus on managing uncertainty, not mitigating it. Therefore, it is important for the designer to identify multiple solutions that are relatively insensitive to uncertainty. The designer will then need to explore the solutions and pick (using human judgement) the best alternative and move forward. They define designing as a conversion of information from needs and requirements of the product into knowledge of the product. A designer should start with

the desired functional requirements and then be able to work backwards to find satisfactory design solutions. Mistree et al. [59] base their work on Simon and Miller [62] who suggest design is decision-based and an artificial science. Their set of DBD beliefs, hypothesis, and knowledge on the work of Miller [63]. They believe design decisions are multileveled and multidimensional in nature. They involve information that comes from different sources and disciplines and may not be complete or available. Some information is "hard", or based on scientific principals while some information is "soft", or based on the designer's judgement/expertise. The lack of information accuracy or completeness leads a designer to make a satisficing decision, or one that is sufficient but less than optimal. One instantiation of DBD is the Decision Support Problem Technique (DSP Technique). The DSP Technique proposed by Muster and Mistree [64] supports a designer in partitioning and formulating design problems in simple terms to assist in finding satisficing solutions. The DSP Technique is implemented in two phases: the meta-design and design phases. In the meta-design phase, the designer is "designing the design phase" and consists of planning and structuring decision support problems. In the actual design phase, the designer finds solutions to the decision support problems and then further verifies or validates the results. We adopt the DSP Technique in this work to embody the goal-oriented, and inverse features of our method. We show the generic form of our goal-oriented, inverse decision-based design method for systems design below in Figure 2.1.

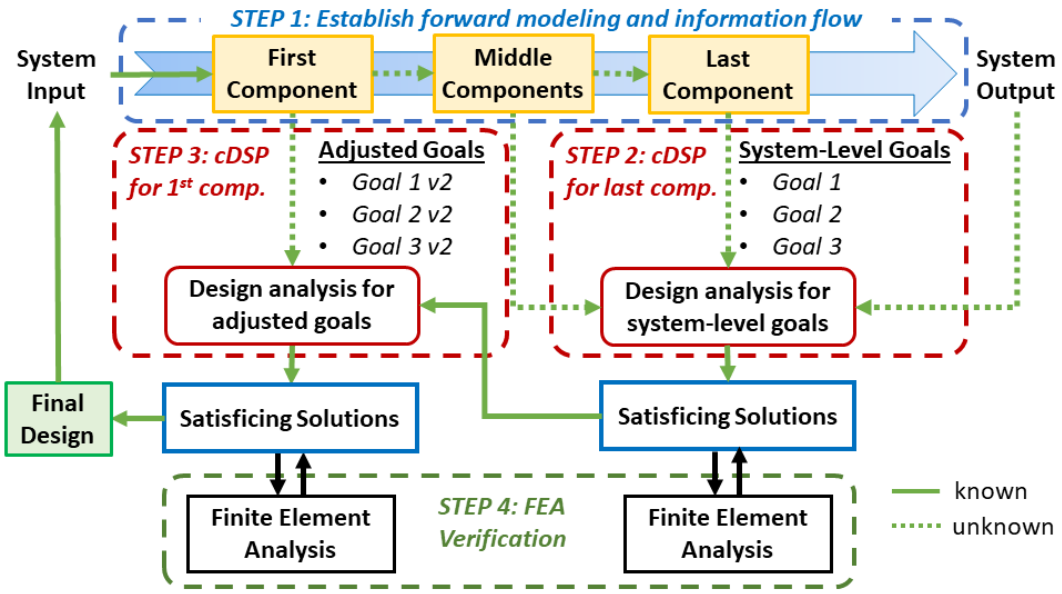

Figure 2.1 The four steps to the generic goal-oriented, inverse decision-based design method for systems design.

At a minimum, the generic form of our method shown in Figure 2.1 requires four essential steps. In Step 1, shown by the blue dashed line, the designer establishes the forward modeling and information flow. Design information is passed into the system and specific requirements are set for the system output. For product design, each conceptual component subject to design is listed in the order information flows from the system input to the system output. The solid green arrow represents "hard" information, and the green dashed arrow represents "soft" information. Information must be mapped in a consistent way, such as matter or energy, from component to component to establish the bottom-up, cause and effect relationships that connect the components to the overall system-level performance requirements. Then, we can establish system-level targets that we use to drive the design of the individual components in an inverse fashion, beginning with the last component in the system.

In Step 2, the designer performs the design analysis to generate a set of satisficing solutions for the final component with respect to the system-level goals. In this step, soft information from the preceding components, design variables and ranges for the current component, and expected behavior at the system level (goals) are used to formulate the design problem. Information about the needs and requirements of the component is converted into knowledge about the component. In Step 3, we pass the new hard information back to design the preceding component. In Figure 2.1, this could be the middle component, or the first component, depending on the number of components subject to design. For each analysis following Step 2, the design requirements are updated so that each set of satisficing solutions will result in a system that at least maintains, if not improves, the system performance. In Step 4, the designer verifies the cDSP results. In product design, this verification may be carried out with FEA, experimentation, or by some other form. Finally, the designer may choose to move on to the embodiment an detailed design phases, or reformulate and repeat the process until a satisfactory system design is achieved.

To systematically collect and manage the information used in Steps 2, 3, etc. we use the Concept Exploration Framework (CEF) construct. We use the compromise Decision Support Problem (cDSP) to find satisficing solutions for our design goals. And to explore the solution space and select a design alternative, we use ternary plots. We discuss the cDSP construct in detail in Section 2.1.1, the CEF construct in Section 2.1.2, and the solution space exploration with ternary plots in Section 2.1.3.

2.1.1 The compromise Decision Support Problem (cDSP)

The cDSP is the foundational mathematical construct used in the analysis steps of our method to find satisficing solutions for each design variable with respect to the conflicting set of system-level goals. McDowell et al. [54] point out that systems design with incomplete and inaccurate models results in different types of uncertainties associated with a system, the design parameters, the math or analysis models, and the uncertainty in their interactions. Therefore, Bras et al. [65] and Mistree et al. [66] formulate the cDSP to find satisficing solutions for the conflicting goals that are insensitive (or robust) to the various forms of uncertainty. The solution space of satisficing solutions can then be explored to make a selection based of the designer's intuition or expertise. The cDSP is a hybrid of mathematical programming and goal programming, where the priority is to achieve a target set for each goal as close as possible. We show the generic form of the cDSP below in Figure 2.2.

GIVEN

An alternative to be improved, domain dependent assumptions

The system parameters:

n number of system variables,

q inequality constraints,

$p + q$ number of system constraints,

m number of system goals,

$g_i(\mathbf{X})$ system constrain functions

$f_k(d_i)$ function of deviation variables to be minimized at priority level k for the preemptive case

FIND

System variables: The values of the independent *system* variables.

X_i $i = 1, 2, \ldots, n$ (They describe the physical attributes of an artifact.)

Deviation variables: The values of the deviation variables.

d_i^-, d_i^+ $i = 1, 2, \ldots, m$ (They indicate the extent to which the goals are achieved)

SATISFY

System constraints: These must be satisfied for the solution to be feasible (linear, non-linear)

$g_i(\mathbf{X}) = 0;\ i = 1 \ldots p$

$g_i(\mathbf{X}) \geq 0;\ i = p+1 \ldots p+q$

System goals: These need to achieve a specified target value as far as possible (linear, non-linear)

$A_i(\mathbf{X}) + d_i^- - d_i^+ = G_i;\ i = 1 \ldots m$

Bounds: Lower and upper limits on the system variables.

$X_i^{\min} \leq X_i \leq X_i^{\max};\ i = 1 \ldots n$

$d_i^-, d_i^+ \geq 0,\ d_i^- * d_i^+ = 0;\ i = 1 \ldots m$

MINIMIZE

A deviation function: A function that quantifies the deviation of the system performance from that implied by the set of goals and their associated priority levels or relative weights.

$\mathbf{f} = [f_1(d_i^-, d_i^+), \ldots, f_k(d_i^-, d_i^+)]$

Figure 2.2 The generic form of the compromise Decision Support Problem [67].

The cDSP has four key sections: given, find, satisfy, and minimize. In the "given" section, the designer lists all the relevant information available about the component. This may include information regarding the system variables, constraints, goals, and targets. In the "find" section, the designer identifies the information about the system variables and

deviation variables to find. The deviation variables d_i^- and d_i^+ represent the underachievement and overachievement from the selected targets G_i. In the "satisfy" section, the designer explicitly lists system constraints, variable bounds, and system goals. Finally, in the "minimize" section, the designer executes the cDSP to minimize the deviation function objective function shown below,

$$Z = \sum_{i=1}^{m} W_i(d_i^- + d_i^+);\ \sum_{i=1}^{m} W_i = 1 \qquad (2.1)$$

where the weights W_i represent the desire to achieve a particular goal. A separate deviation function is written to minimize for each system level goal. The designer exercises the cDSP to generate a set of satisficing design variable solutions according to a weight sensitivity analysis that will be discussed in detail later.

2.1.2 The Concept Exploration Framework (CEF)

The second core construct to our goal-oriented, inverse decision-based design method is the Concept Exploration Framework (CEF) proposed by Nellippallil et al. [55]. In our method, we use the CEF in each step to systematically collect the information needed complete and exercise the cDSP. The CEF is derived from the Robust Concept Exploration Framework (RCEF) developed by Chen et al. [68]. The generic form of the CEF is shown below in Figure 2.3.

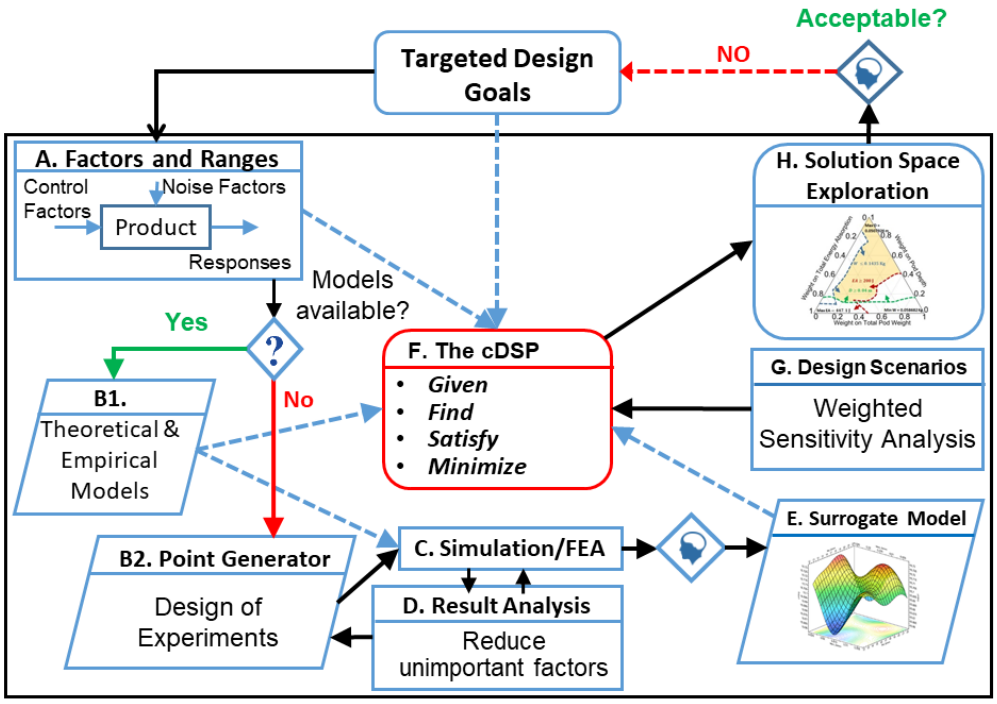

Figure 2.3 The generic Concept Exploration Framework (CEF) for collecting and managing design information.

The generic CEF shown in Figure 2.3 above includes eight processors (A, B1, B2, D, E, F, G, H) and simulation programs (C). At the heart of the framework is the cDSP computational framework described in Section 2.1.1. Essentially, the framework is useful for collecting and managing the necessary design information to then generate a set of satisficing solutions and make decisions under the assumption that the information is not complete or completely accurate. To start, the selected design goals and targets defined during the problem formulation (see Figure 2.1, Step 1) can either come from the "end", at the system-level, or from the top down in the form of adjusted goals and targets. Design goals and targets information, along with the information collected through Processors A, B1, B2, C, D, and E are passed directly into the cDSP. In Processor A, the designer identifies the design factors (variables) and establishes the ranges (lower and

upper bounds). If there are theoretical or empirical models available to describe the design variables in terms of the system level goals, then the information is passed from Processor B1 into the cDSP. If no theoretical or empirical models are available, then the designer must iterate through processors B2, C, and D to gather data from a DOE in Processor B2, a simulation or analysis program in Processor C, and refinement in Processor D. The information collected from Processors B2, C, and D is passed on to Processor E to create a surrogate model. The surrogate models are passed directly into the cDSP and the preliminary information collection process is complete. The designer can exercise the cDSP (Processor F) to find satisficing solutions for the design variables with the weight sensitivity analysis in Processor G, and then explore the solution space in Processor G. In this thesis, we use ternary plots to explore the solution space and find satisficing solutions.

2.1.3 Solution Space Exploration with Ternary Plots

The weight sensitivity analysis and solution space exploration Processors G and H, respectively, is carried out with ternary plots. In this thesis, we only define three goals for our system. Therefore, in Processor G, we need to vary weights on the three goals, which are plugged directly into the three minimization functions in the cDSP. We show the weighting scenarios for a three-goal problem in Table 2.1 below.

Table 2.1 Concept Exploration Framework Processor G weight scenarios for a three-goal problem formulation.

Scenarios	W_1	W_2	W_3
1	1	0	0
2	0	1	0
3	0	0	1
4	0.5	0.5	0
5	0.5	0	0.5
6	0	0.5	0.5
7	0.25	0.75	0
8	0.25	0	0.75
9	0.75	0	0.25
10	0.75	0.25	0
11	0	0.75	0.25
12	0	0.25	0.75
13	0.33	0.34	0.33
14	0.2	0.2	0.6
15	0.4	0.2	0.4
16	0.2	0.4	0.4
17	0.6	0.2	0.2
18	0.4	0.4	0.2
19	0.2	0.6	0.2

The weights range from 0 to 1 where a value of 1 represents the highest preference, and a value of 0 represents no preference. Scenarios 1-3 represent a maximum weight assignment to find design solutions that satisfy the design requirements and achieves a goal as close as possible with no preference on the other goals. Scenarios 4-6 split the preference between two goals equally, while giving no preference to the third goal. Scenarios 7-12 give a higher preference to one goal, a low preference to another goal, and no preference to the last goal. Scenario 13 represents an equal preference split among the three goals. Scenarios 14-19 distribute the preference among the three goals in different amounts. Exercising the cDSP for all 19 weight assignments gives the minimum number of design alternatives needed to span the ternary design space shown in Figure 2.4 below.

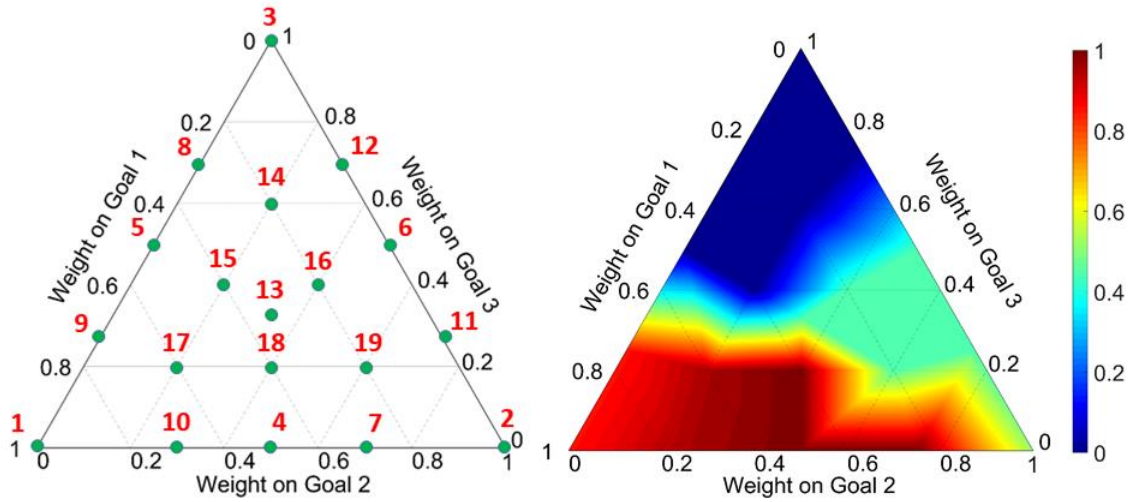

Figure 2.4 A blank ternary plot (left) with the distribution of 19 design points and a colored ternary plot (right) used to visualize the 19 normalized solution values for the three design goals.

On a ternary plot, the three axes represent our three design goals, where the axis range from 0 to 1 represents the normalized maximum and minimum goal values, respectively. In the blank ternary plot, shown on the left in Figure 2.4 above, the green points are the 19 design points from the weight sensitivity analysis. Wang et al. [69] propose a systematic method for exploring the ternary plot solution space. To visualize the solution space with the colored plot shown on the right in Figure 2.4, we can plug the design variables into the goal formulations (theoretical, empirical, or surrogate models) to calculate the real goal values. Then, the goal values must be normalized on a scale of 0 to 1 to be plotted and then compared against the other goals where a dark red color represents a maximum value of 1, and dark blue represents a minimum value of 0. All design points are technically feasible design points but may not satisfy the designer's preference. Therefore, the designer can now specify a preference boundary that reduces the design space to make selection easier. Three colored plots must be generated, one

with respect to each goal, and then combined as one plot to reveal the satisficing solution space. The designer can now select from the available satisficing solutions or reiterate to expand or reduce the number of options.

2.1.4 Next Steps to Use the Goal-Oriented, Inverse Decision-Based Design for Helmet Design

The goal-oriented, inverse decision-based design method with the cDSP and CEF design constructs and ternary plot tool discussed thus far were first demonstrated to design materials and the associated manufacturing hot rod rolling processes by Nellippallil et al. [55, 67, 70-73]. In this thesis, we adapt their framework for product design and lay the foundation for the design of multiple football helmet components. First, we demonstrate the design of a simplified helmet liner to verify the applicability of the CEF, cDSP, and ternary plots for helmet design. Then, we demonstrate the design of two components: the actual helmet liner with respect to the system-level goals, and then the composite shell with respect to modified goals to establish the efficacy of our selected method for system design. In both examples, we frame the problem to follow a helmet strike that transfers energy through the composite shell, into the foam liner, and then into the head. From a helmet design perspective, we desire three key functionalities, namely, to absorb impact energy, minimize system weight, and mitigate stress waves. From these goals, we can define performance targets and set design constraints at the system level. At the sub-system level, each individual component has unique objectives, constraints, and variables that describe the design variables. A major challenge in our work is in establishing a proper flow of information that allows us to design the components with respect to each other and the system-level goals. We find that all helmet components play

different roles in managing the impact energy and both affect the overall system weight. Therefore, setting the performance goals in terms of energy and mass allows us to establish a proper forward flow of information.

In Section 2.2, we detail the design of a simplified version of the foam liner using the CEF, cDSP, and ternary plots. Then, in Section 2.3, we detail the design of two subassemblies, namely, the helmet composite shell, and the foam liner to demonstrate the full functionality of our method.

2.2 Demonstrating Our Method to Design the Foam Liner Composed of Six Cylindrical Foam Pods Wrapped in Thermoplastic Polyurethane

In this section, we demonstrate our goal-oriented, inverse decision-based design method with the cDSP, the CEF, and solution space exploration with ternary plots to design a simplified version of the helmet region foam liner and TPU wrap. Our interest in this exercise does not lie in the results, rather in establishing confidence in the applicability of the constructs and solution space exploration tool for helmet design.

2.2.1 Problem Definition

A typical American football helmet comprises six regions (excluding the facemask) including the front, side, front boss, rear boss, rear, and top. With respect to helmet design, we believe a good helmet should provide protection for the different player positions which may need greater levels of protection in some regions, and not in others. For example, a lineman may need more protection at the front of the helmet, where a wide receiver may need protection at the top, side, or rear. Therefore, the overall goal is to design the different regions of the helmet with our inverse method, but in this section, we focus only on the top region. To make our analysis simple, we use a flat

representation of the top region that has approximately the same surface area as the real helmet region. We show a diagram of our helmet section and simplified geometry in Figure 2.5 below.

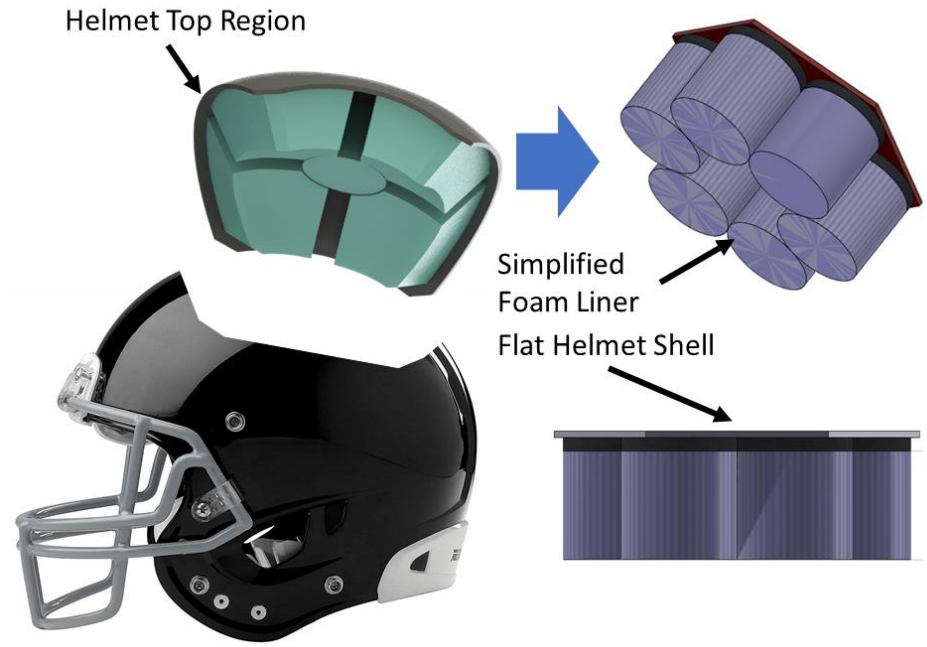

Figure 2.5 Example top region and simplified region featuring a flat shell and 6 cylindrical foam pods wrapped in thermoplastic polyurethane.

The simplified, flat region shown in Figure 2.5 above was inspired by the experimental design work of Rush et al. [48]. In their work, which we discussed in Section 1.3, the optimal foam liner design consist of SunMate (Dynamic Systems Inc.) Firm Foam (84.3 kg/m^3) cylindrical pods, wrapped in a thermoplastic polyurethane (TPU) film, and covering approximately 75% (AR = 0.75) of the head. We compared different flat section geometries but found a hexagon shape was the only base shape that allowed equal pod spacing and 75% coverage. We position 6 TPU wrapped foam cylinders in a circular array with no preference to the cylinder diameter. In this analysis,

we left a space in the center of the array to incorporate a stress wave damper in future work. The hexagon base shell had a surface area of 18763.47 mm^2 and each of the 6 foam cylinder had a fixed cross-sectional diameter of 53.88 mm making the combined surface area of the foam 13680.32 mm^2. The ratio of the foam cylinder surface area to the base hexagon shell surface area was 0.73, which is within 3% of our target AR of 0.75. In the design analysis, we only considered two design variables, namely, the foam pod depth and the TPU wrap thickness. We show both design variables and their ranges in Table 2.2 below.

Table 2.2 Foam liner design variables and ranges for the simplified liner design.

	Minimum	**Maximum**
Pod Depth (D) (mm)	25.4	50.8
TPU Thickness (t) (mm)	0.1	1.30

We strike the top of the foam with a 5 kg mass and 5.46 m/s velocity, which correspond to the NOCSAE standard headform mass and the final velocity from a 5 ft. standard NOCSAE twin-wire drop tower test, respectively. We set three goals for our liner component, namely, to maximize energy dissipation (Goal 1), minimize component weight (Goal 2), and maximize the pod depth (Goal 3). Goal 1 is measured with internal energy (J), and our target of 100% dissipation would be achieved if the system completely traded the impact kinetic energy for internal energy. Therefore, our target for internal energy is equivalent to the input kinetic energy, or 74.53 J. However, we realize this target may be impossible to achieve and we expect the actual internal energy result will be less than the target. We set a lower bound for internal energy at 37.26 J, based off our intuition, to constrain the system to at least 50% dissipation. The combined weight of the foam cylinder and TPU wrap makes up Goal 2. We set the Goal 2 weight target as the

minimum possible weight from the combination of design variables (See Table 2.2). For an array of 6 pods, the weight target for Goal 2 is 0.034 kg with a maximum constraint of 0.2 kg. that corresponds to the combination of maximum design variables. We measure Goal 3 pod depth as the normal distance from the shell to the base of the foam pod. Typical football helmet liners are approximately 38.1 mm (1.5 in.) deep, however we want to explore a range of options because Rush et al. [48] found that pod depth (liner depth) had the greatest influence on energy absorption. Therefore, we set the depth target at 50.8 mm with a minimum depth greater than 25.4 mm. Our minimum value of 25.4 is the minimum depth allowable to protect the head from the hard shell at the onset of foam densification. It is important to note that these three design goals are conflicting in nature, where a larger pod depth or thicker TPU thickness may help Goals 1 and 3 but hurt Goal 2. Therefore, we rely on the solution space exploration, enabled by our ternary plot tool, to find overlapping satisficing design regions. This is a very simple design problem; therefore, we are not interested in the results, but rather in successfully exercising the CEF, the cDSP, and ternary plot tools to verify they are appropriate for our future helmet design. In the next section, we describe the CEF and cDSP to find satisficing solutions for our foam liner and TPU wrapped pods.

2.2.2 The Concept Exploration Framework and compromise Decision Support Problem to Design the Simplified Liner Subsystem

In this problem, we use the CEF to manage information collection, design analysis, and solution space exploration. We show the CEF with the specific input targets and processors needed to design the simplified foam liner in Figure 2.6 below.

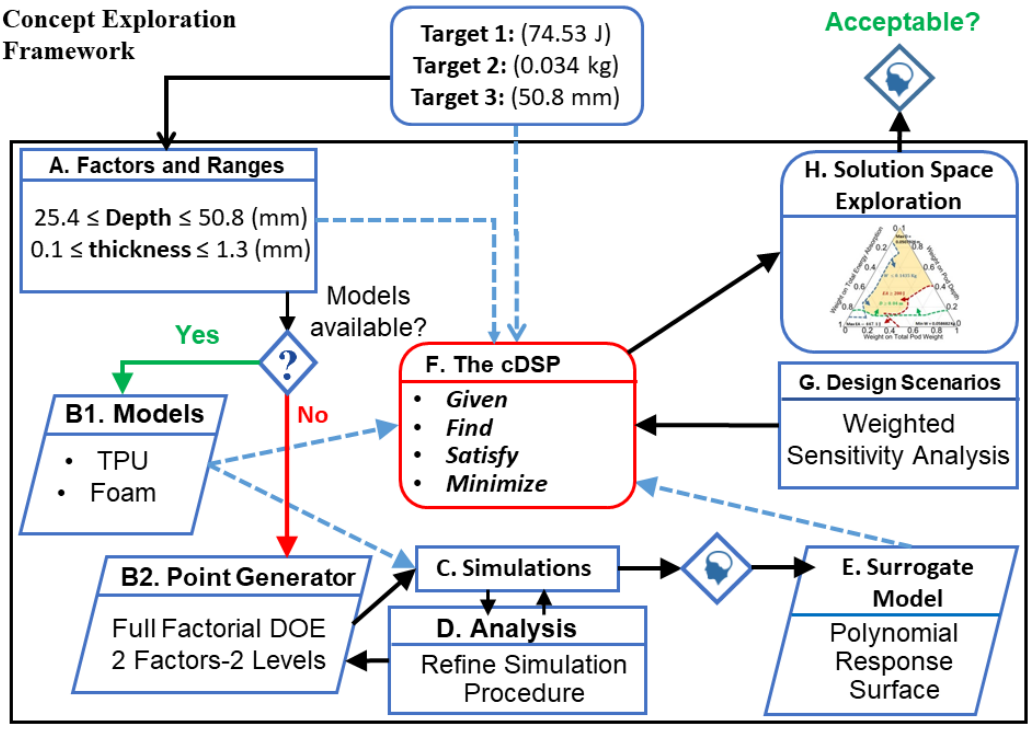

Figure 2.6 The Concept Exploration Framework (CEF) for the simplified foam liner subsystem.

As we mentioned in Section 2.2.2, the CEF is composed of data collection processors: A, B1, B2, D, & E, simulation processor C, and design analysis processors: F, G, & H. Targets 1, 2, and 3 are the specific values we wish to attain from our three design goals. We pass this information directly into Processor F, the cDSP, and Processor A. In processor A, we define the variable ranges for our two design factors, namely, foam pod depth (D) and TPU wrap thickness (t). Next, we find or create the math models that describe our liner subsystem. Because we simplified the geometry and design variables, we can easily calculate the subsystem weights and pod depth with simple analytical calculations in processor B1. The analytical model for system weight is shown below.

$$Wt(D,t) = 6 * [(m_{TPU} * V_{TPU}) + (m_{foam} * V_{foam})] \quad (2.2)$$

Where m_{TPU} is the mass of the TPU wrap, m_{foam} is the mass of the foam, V_{TPU} and V_{foam} represent the volume of the TPU wrap and the foam, respectively. We calculate V_{TPU} with the equation below.

$$V_{TPU}(D) = \left(\pi * \frac{d_{pod}}{2} * D\right) - V_{foam} \tag{2.3}$$

Where $d_{pod}$is the outer diameter of a cylindrical liner pod, and D is the pod depth design variable. We calculate $V_{foam}$with the equation below.

$$V_{foam}(D, t) = \pi * \left(\frac{d_{pod}}{2} - t\right) * (D - 2 * t) \tag{2.4}$$

Where $d_{pod}$is the outer diameter of a cylindrical liner pod, D is the pod depth design variable, and t is the TPU thickness design variable. Next, we need to create a metamodel that describes energy dissipation in terms of our two design variables. Therefore, we use processors B2 to create a Design of Experiments (DOE), processor C and D to run Finite Element Analysis (FEA), and processor E to create a polynomial response model from the FEA results. Because we only have two factors and two levels (2^2), we can easily construct and run analysis on a full factorial DOE with 4 runs. We show the full factorial DOE for the foam liner subsystem in Table 2.3 below.

Table 2.3 Four level (2^2) full factorial Design of Experiments (DOE) for the simplified foam liner subsystem Internal Energy.

Experiment	Depth (mm)	Thickness (mm)
1	25.4	0.1
2	25.4	1.3
3	50.8	0.1
4	50.8	1.3

We construct a quarter-pod Finite Element mesh and strike top with a rigid flat plate using the prescribed boundary conditions mentioned earlier. A description of the

Finite Element Analysis will be given in the next section. From the FEA results, we constructed the polynomial response model for internal energy in terms of our two design variables. The polynomial response model is shown by the equation below.

$$IE(D,t) = ((0.0063(D) + 0.3933(t) - 3.8701(D) * (t)) * 10\text{^}5) \quad (2.5)$$

Where D and t are the design variables for pod depth and TPU thickness, respectively. The design information collected through CEF processors A-E can now be used to formulate the cDSP. As we described in Section 2.1.1, the formal cDSP has for key sections: *Given, Find, Satisfy, and Minimize*. We show the formal cDSP for our simplified foam liner subassembly below.

Given:

(1) The three performance goals identified for our simplified foam liner subassembly

- Maximize internal energy (IE)
- Minimize system weight (Wt)
- Maximize pod depth (D)
- Achieve target energy dissipation (100%)
- Target value for internal energy, IE = 74.53 J
- Target value for system weight, Wt = 0.034 kg
- Target value for pod depth = 50.8 mm

(2) The foam liner polynomial response models

- Internal energy (IE), see Equation #
- TPU Volume, see Equation #
- Foam Volume, see Equation #
- System weight, see Equation #
- Pod Depth

(3) Variability in system variables

We provide the system variables in the *Find* and *Satisfy* sections.

Find:

System Variables

X_1, foam depth (D) – 25.4 to 50.8 mm

X_2, TPU thickness (t) – 0.1 to 1.3 mm

Satisfy:

System Constraints

- Minimum Internal Energy Constraint

$$IE \geq 37.3\,J \tag{2.6}$$

- Maximum Weight Constraint

$$Wt \leq 0.2\,kg \tag{2.7}$$

- Minimum Depth Constraint

$$D \geq 25.4\,mm \tag{2.8}$$

System Goals

Goal 1:

- Maximize Internal Energy

$$\frac{IE(X_i)}{IE_{Target}} + d_1^- - d_1^+ = 1 \tag{2.9}$$

Goal 2:

- Minimize System Weight

$$\frac{Wt_{Target}}{Wt(X_i)} - d_2^- + d_2^+ = 1 \tag{2.10}$$

Goal 3:

- Maximize Pod Depth

$$\frac{D(X_i)}{D_{Target}} - d_3^- + d_3^+ = 1 \tag{2.11}$$

V*ariable Bounds*

X_1 – 25.4 to 50.8 mm

X_2 – 0.1 to 1.3 mm

Bounds on deviation variables

$$d_i^-, d_i^+ \geq 0 \text{ and } d_i^- * d_i^+ = 0, i = 1,2,3 \tag{2.12}$$

Minimize:

We minimize the deviation function.

$$Z = \sum_{i=1}^{3} W_i(d_i^- + d_i^+); \sum_{i=1}^{3} W_i = 1 \tag{2.13}$$

We formulate the cDSP (shown above) in CEF processor F, and then run it 19 times according to a weight sensitivity analysis in processor G to obtain 19 design points. In the last CEF processor H we plot the design points with a ternary plot and then explore the solution space to find satisficing solutions for each of our design goals. Finally, we can make our design decisions. In the next section, we review the FEA used to develop the internal energy metamodel.

2.2.3 Finite Element Analysis

To develop a metamodel for internal energy, we only needed 4 simulations from a 2 factor, 2 level (2^2) DOE. We created each mesh for the DOE and ran the impact simulations in Abaqus Explicit. To simplify the computations, we modeled only a quarter of one foam pod with TPU wrap and applied symmetric boundary conditions on both symmetry faces. We conducted a mesh refinement study for the foam and TPU components. To select a mesh for the foam, we conducted two refinements where we increased the number of elements in one study, and then increased the order of elements in the next study. Both refinement studies had seven iterations where we measured von Mises stress at the fixed surface and internal energy. In the first refinement, we uniformly increased the number of elements by decreasing the global seed size from 4.5 down to 1.0. In the second refinement, we increased the order of interpolation from linear to quadratic. We found a maximum of 0.88% change in von Mises stress across all seven iterations in both refinements. Therefore, we selected the elements with a seed size of 3 mm and linear interpolation based on CPU time.

We conducted a similar refinement to determine the appropriate mesh for the 0.1 mm thick TPU shell elements. However, in addition to increasing the number of elements and order of interpolation, we also compared the results from triangular (S3R) shell elements. In this refinement study, we tracked changes in artificial energy, internal energy, and total energy. We found that shell elements tend to increase the total energy of the system due to higher than normal artificial energy that results from hourglassing errors. We found we could mitigate the hourglassing errors either with quadratic elements, or a larger number of linear elements. We selected linear interpolation, square

elements at a seed size of 0.8 based on CPU time. There was no difference in answer when comparing the selected mesh to that of a triangular (S3R) mesh. In the two analysis with 1.3 mm thick TPU, we used with explicit C3D8R continuum brick elements. We ensured the total energy, artificial energy, and internal energy values were consistent with the results from the refinement study and selected seed sizes to ensure all aspect ratios were below 3. We fixed a rigid flat plat made of R3D4 elements at the base of the pod and placed another plate approximately 1 mm above the top of the foam pod. In Table 2.4 below we show the final mesh details for the quarter symmetry pod.

Table 2.4 Finite element analysis mesh details for the quarter symmetry pod wrapped in thermoplastic polyurethane.

Component	**Element Type**	**# of Elements**	**# of Nodes**
Plate	R3D4 – rigid, linear, quadrilateral	100	121
Foam	C3D8R – linear brick & reduced integration	1760 – 3840	2208 - 4600
TPU Shell	S4R – 2D shell with reduced integration	3942 – 5616	3942 - 5748
TPU Solid	C3D8R – linear brick & reduced integration	12500 - 17200	16080 - 22080

We placed a reference point at the center of the upper plate that we used to apply a 5 kg mock headform mass and -5.46 m/s impact velocity. We allowed the analysis to run long enough for the rigid plate to compress the quarter symmetry pod and then completely relax. We use two materials in this analysis, a viscoelastic TPU model for the wrap and low density foam model for the foam. We modeled the viscoelastic TPU model with Prony series time constants provided by Zhou, et al. [74]. We also used their values

for density, and Poisson's ratio that were 1070 kg/m^3 and 0.485, respectively. We used the low-rate (0.1/s) and high-rate (600/s) compression test data collected by Rush et al. [48] with the Abaqus low density foam model and a density of 84.3 kg/m^3 and Poisson's ratio of 0.1 to model the SunMate (Dynamic Systems Inc.) Firm foam. We show both material models below in Figure 2.7.

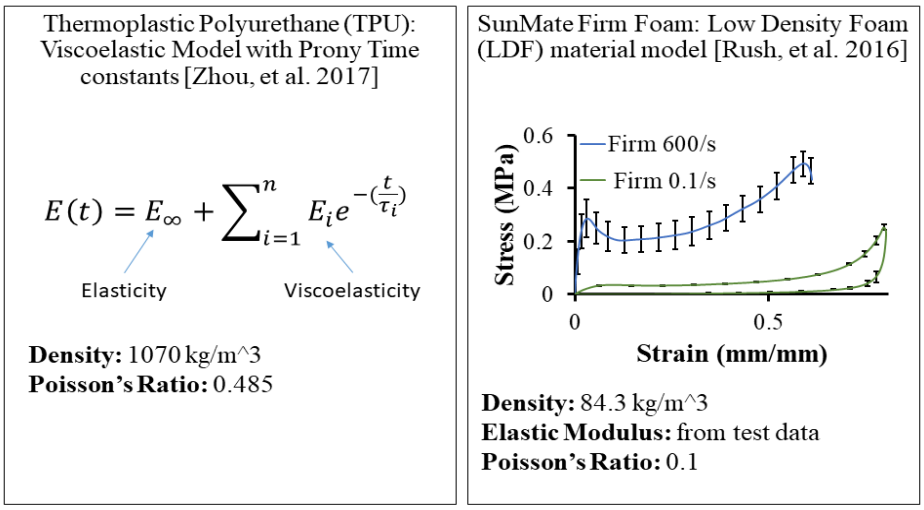

Figure 2.7 Viscoelastic TPU model (left) and SunMate (Dynamic Systems Inc.) Firm foam low density foam model from experimental data (right).

Through the analysis time history, we see an inverse correlation between kinetic energy and internal energy. At the start of the analysis, kinetic energy is at its highest, and internal energy is at its lowest and then we see a total tradeoff at the point where the pod is fully compressed. Then the pod relaxes and returns to equilibrium where we see the kinetic energy value is much lower due to the dissipated energy. We take the value of internal energy at equilibrium as the measure of energy dissipated by our pod. We find different levels of internal energy for the four different analysis that we use to create our metamodel.

2.2.4 Solution Space Exploration and Discussion

In this section, we describe the integrated solution space exploration of the simplified foam pods to verify our ternary plot tool. We exercise the cDSP according the CEF Processor G weight sensitivity analysis discussed in Section 2.1.3. The weights range from 0 to 1 where a value of 1 represents the highest preference, and a value of 0 represents no preference. Scenarios 1-3 represent a maximum weight assignment to find design solutions that satisfy the design requirements and achieves a goal as close as possible with no preference on the other goals. For example, with Scenario 1, we find a solution for the pod depth and TPU thickness that lie within the specified constraints and achieves the internal energy target as close as possible with no preference to weight or depth. Scenarios 4-6 split the preference between two goals equally, while giving no preference to the third goal. Scenarios 7-12 give a higher preference to one goal, a low preference to another goal, and no preference to the last goal. Scenario 13 represents an equal preference split among the three goals. Scenarios 14-19 distribute the preference among the three goals in different amounts. Exercising the cDSP for all 19 weight assignments gives the minimum number of design alternatives needed to span the ternary design space.

As we discussed in Section 2.1.3, a ternary plot has three axes that represent our three design goals, and the axis range from 0 to 1 represents the normalized goal value. We evaluate the cDSP at each point, and then get a set of design variables which we plug into the polynomial response models to calculate the goal values. The goal values must be normalized on a scale of 0 to 1 to be plotted and then compared with the other goals to find a satisficing region. In our analysis, our objectives were to maximize internal energy,

minimize weight, and maximize pod depth. Therefore, we desire a normalized solution of 1 for the internal energy and pod depth goals and 0 for the weight goal because we desire the maximum and minimum values, respectively. After creating the 19 design points, we visualize the solution space by assigning color values to the normalized solutions where a dark red color represents a maximum value of 1, and dark blue represents a minimum value of 0. Then, we can draw boundaries on each plot based on our preference. To visualize all three goals we generate four ternary plots, one to show the goal attainment for each of the three goals, and the fourth reveals the overlapping, or satisficing, region. We show the four ternary plots in Figure 2.8 below.

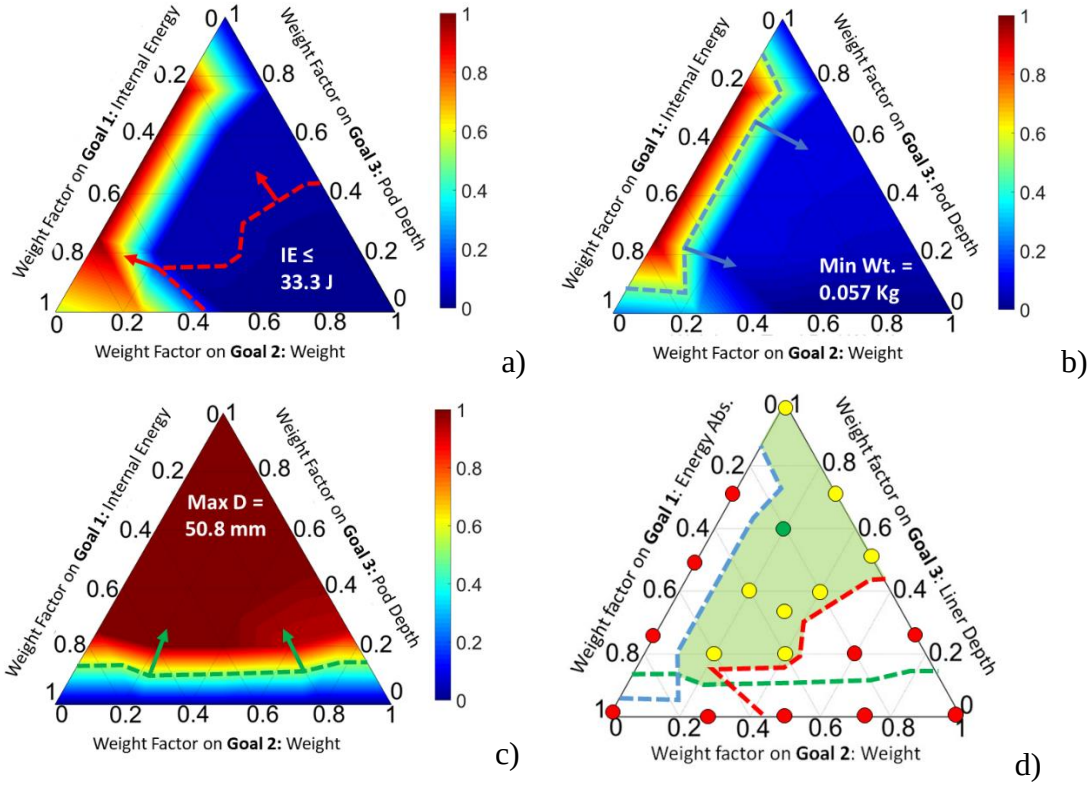

Figure 2.8 Ternary plots showing the goal attainment for a) internal energy (Goal 1), b) weight (Goal 2), c) pod depth (Goal 3), and d) the satisficing solution space.

In Figure 2.8-a, we see the relative attainment with respect to the internal energy Goal 1. Because our goal was to *maximize* internal energy, we search for solutions in the red region. However, as we can quickly see from the color contour, if we limited the solution space to the red region alone, that would severely limit our number of design alternatives. Therefore, we relax our preferences a bit to open up the design space and allow any design with at least 33.3 J of internal energy. In Figure 2.8-b, we see the relative attainment with respect to weight, Goal 2. As our goal was to *minimize* system weight, we look for solutions in the dark blue regions. Thankfully this includes most of the design space and we do not need to relax our preferences. In Figure 2.8-c we the attainment for pod depth, Goal 3, and again most of the space is acceptable and we do not need to relax our preferences. In Figure 2.8-d, we see the overlapping, or satisficing solution space that contains all the design points that satisfy our three design goals. There are 9 alternatives for selection, however they are all very similar, therefore we simply choose the design with the largest internal energy value. The final design point number 14, shown as the green dot in Figure 2.8-d, had only 34 J internal energy, a system weight of 0.066 kg, and a pod depth of 50.8 mm. In this problem, we are not interested in the results, but rather exercising our design constructs and solution space exploration tools to verify their use for product design. Now that we understand the cDSP, the CEF, and ternary plot tool, in the next section, we use them to design two components together with respect to the same set of system-level goals.

2.3 Demonstrating Our Method To Design Two Helmet Components

In this section, we use the same method and constructs demonstrated in the previous example but here we demonstrate the full functionality by designing two

components. We design the foam liner and the composite shell from the actual helmet prototype to establish the efficacy of our goal-oriented, inverse decision-based design method for systems design.

2.3.1 Helmet Region Problem Description

The example from the previous section confirmed the cDSP, CEF, and ternary plot tool we selected for our inverse design method. However, the flat test section was a gross simplification of the real football helmet and the results do not provide insight into the helmet functionality. In this section, we take another step towards our ultimate goal of designing the entire helmet and make two key improvements from the previous work. First, we use realistic geometry from a region taken directly from the prototype helmet. Second, we demonstrate the design of two components with respect to the same set of system level goals. We only need to design two components to demonstrate the forward information flow, model integration, and goal-oriented inverse decision-based design. In the future we can build on this work again to add additional components or alter the design goals and requirements to design the final helmet section.

Until we are able to quantify the exact mechanisms that cause MTBI, we assume that a football helmet must have a high-energy absorption capacity, an ability to mitigate stress waves, and a minimum total weight to lower the risk of MTBI. In terms of our problem definition, these key performance characteristics translate to three system-level goals, namely, to dissipate the kinetic energy (Goal 1), minimize total system weight (Goal 2), and to mitigate the stress waves (Goal 3). We formulate Goal 1 in terms of internal energy and our goal is to achieve the target value of 100% energy dissipation. In other words, the system completely transformed the kinetic energy into internal energy.

In reality, it might be nearly impossible to achieve the target, but with our framework we can still find a design that achieves our goal with a minimum deviation from the target. We formulate Goal 2 in terms of mass and our goal is to achieve the minimum possible weight our design constraints allow. We measure stress wave mitigation, Goal 3, by taking the time integral of the reaction force at the interface between the foam and head. The time integral of the reaction force is formally called the impulse, with units of Newton*seconds (N*s) and is a measure of the stress history multiplied by the surface area of the foam.

Ideally, to design a helmet region, we would have a collection of actual game data that we could use to model boundary conditions and set performance targets specific to player position. However, at this time we are more interested in demonstrating the method, therefore we continue to use the current industry standard test metrics provided by NOCSAE. We select the standard test method for testing newly manufactured football helmets in the top position by means of a twin-wire drop test [8]. We use FEA to simulate an impact normal to the surface of the shell using the prescribed boundary conditions listed in the NOCSAE standards. We used data collected from the FEA to build metamodels that we use in the cDSP to generate design alternatives under uncertainty. The scope of our design study is limited to the foam liner and composite shell only, and as we mentioned earlier, we select the top region of the helmet for design exploration because it is known be one of the more dangerous helmet regions with respect to brain injury [25, 26, 48]. Figure 2.9 below shows the top helmet region used in this study.

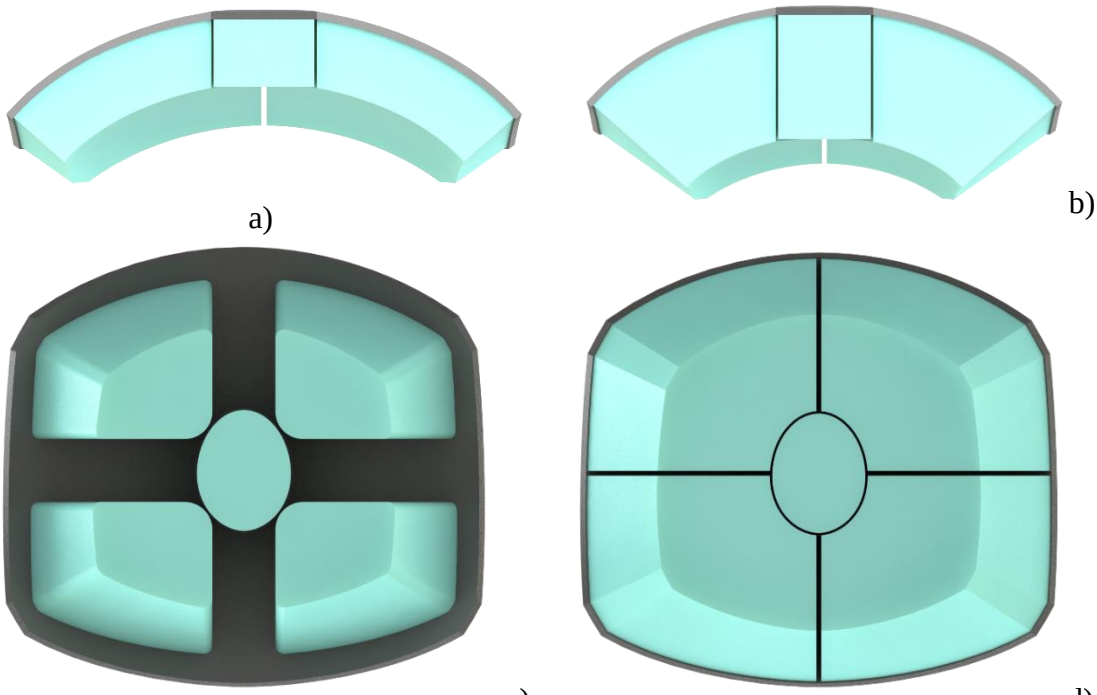

Figure 2.9 Top helmet region showing a) the minimum foam depth (25.4 mm), b) the maximum foam depth (50.8), c) the minimum area ratio (AR = 0.5), d) the maximum area ratio (AR = 1.0).

In Figure 2.9, we show the top helmet region at the minimum and maximum configurations in a/b and c/d, respectively. The foam liner design variables are taken from Rush et al. [48] who determined the foam depth, area ratio (AR), foam density, and input kinetic energy were among the primary factors that affect energy dissipation. The foam depth is measured as the normal distance from the inside of the shell. Our minimum foam depth is 25.4 mm, maximum foam depth is 50.8 mm, with a constraint on the maximum foam compression distance cannot exceed 50% of the original value. For example, if the original foam depth were 38.1 mm, the maximum compression cannot exceed 19.05 mm (38.1 – (0.5*38.1)). The Area ratio (AR) is the ratio of foam surface area to head surface area. The minimum AR is 0.5 and maximum AR is 1.0 that represents 50% and 100% coverage, respectively. We select three foam options from

Rush et al.'s experimental work. All three options are made by SunMate (Dynamic Systems Inc.) and vary in density from Medium (79.9 kg/m^3), to Medium-Firm (82.8 kg/m^3), to Firm (84.3 kg/m^3). Rush [48] was limited to the foam cylinder design by in-house manufacturing capabilities, however we suspect trapezoidal or pyramid shapes would be better suited for helmet curvature and fill the gaps between the head and the outer shell. Therefore, we maximize the foam volume while maintaining the same design parameters (depth, density, and AR). These trapezoidal 'block-like' shapes are common to helmets and could easily be injection molded for the final helmet design. Finally, we represent the input kinetic energy as a velocity because our impacting mass remains constant. We calculated the final velocity from free-fall at 2, 3, and 4 ft. heights as our input velocity. In the shell design study, we use shell thickness and density as our design variables. The shell thickness has a minimum and maximum value of 1 mm and 5 mm respectively. The shell density is taken to be composite density of a polypropylene (PP) base with short E-glass fibers added in volume fractions (VF) ranging from 10% to 50%. We select the 10% E-glass VF as our minimum and 50% VF as our maximum, corresponding to composite densities from 970 kg/m^3 to 1330 kg/m^3, respectively. In Table 2.5 below we show the design variables and their respective ranges for the foam liner and composite shell.

Table 2.5 Composite shell and foam liner design variables and ranges.

	Minimum	Median	Maximum
Foam depth (mm)	25.4	38.1	50.8
AR	0.5	0.75	1.0
Foam Density (kg/m^3)	79.9	82.8	84.3
Velocity (m/s)	3.46	4.24	4.89
Shell thickness (mm)	1	3	5
Shell density (kg/m^3)	970	1120	1330

In the next section, we describe the four steps to our method and show the cDSP for both components.

2.3.2 The Concept Exploration Framework and compromise Decision Support Problem to Design the Helmet Region

In this section, we detail the four steps to our goal-oriented, inverse decision-based design method with special emphasis on the CEF and the cDSP. We show the goal-oriented, inverse decision-based design method formulated for helmet design in Figure 2.10 below.

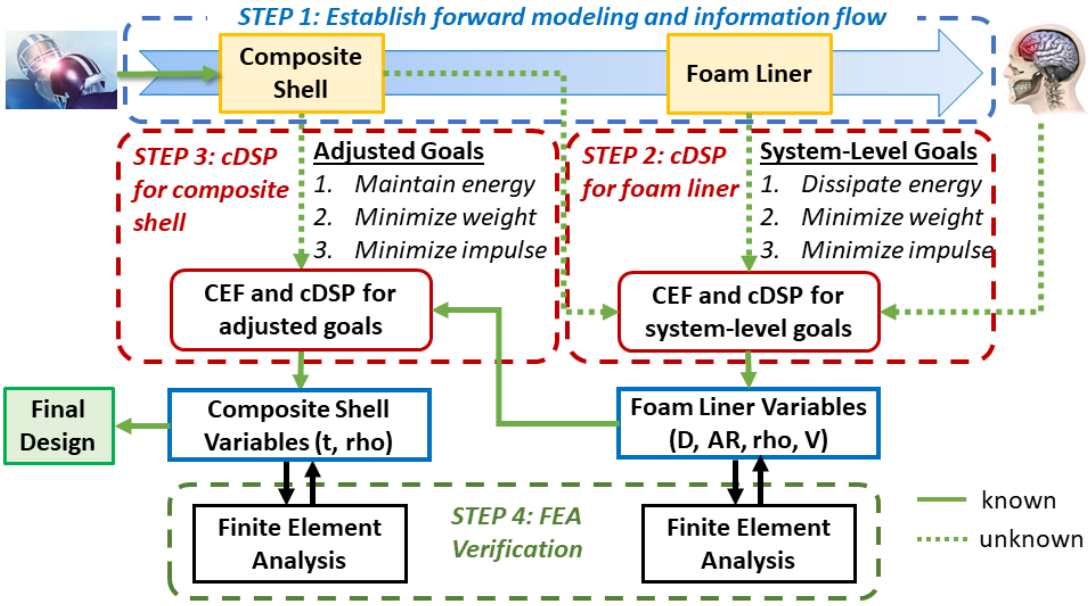

Figure 2.10 The four steps required to design two helmet components with the goal-oriented, inverse decision-based design method.

The first step in the method shown in Figure 2.10 is to establish a forward flow of information that links each component to the system-level goals in a consistent way. To establish the "forward modeling and information flow" (shown by the thick blue arrow) we track the energy transferred from a helmet impact, through the composite shell, through the foam liner, and then into the player's head. The green dashed arrow represents soft information about a component, to be determined in the design analysis. Solid green arrows represent our known design information, or "hard information." The foam liner and composite shell differ greatly in form and function, however must be represented in such a way that ensures a proper flow of information. To do this, we create metamodels that describe the three system-level goals in terms of the individual component design variables. Then we can find satisficing solutions for one component, and then pass hard information back to design another component in an inverse fashion. In Step 2, we use the CEF and cDSP to find satisficing solutions for the foam liner that

achieve the 3 system-level goals as close as possible. All the design information going into the analysis at this point, represented by the dashed green arrows, is soft information. After the analysis, we verify the design decisions with FEA, and then modify our design goals, constraints, and targets. In Step 3, we pass hard information back to design the composite shell with respect to modified design goals. In Step 4 we verify all design solutions with FEA.

In Steps 2 and 3, we manage the design information with the CEF and generate satisficing solutions under uncertainty with the cDSP. Recall the generic formulation of the CEF in Figure 2.3. The process begins by identifying the system-level performance goals and targets that relate to individual components. Then, we work through the Processors, from A to E, collecting information for the cDSP. After the metamodeling in Processor E is complete, we feed all the required information into the cDSP (Processor F) and run to complete Processors G and H. Processors G, H allow the designer to explore the solution space with multiple design points generated with the cDSP and a weight sensitivity analysis. Finally, the designer can make decisions from the available satisficing solutions and determine if the solutions are acceptable through verification or other means. The cDSP consists of four key sections: given, find, satisfy, and minimize. In the "given" section, the designer lists all the relevant information about the system parameters such as the number of system variables, constraints, goals, constraint functions, goal functions, and goal targets. Then the designer may specify the variables they want to "find", the system constraints the variables must "satisfy" and deviation functions that must be "minimized." We give more details regarding the formulation and

utility of the cDSP and CEF in Sections 2.1.1 and 2.1.2, respectively. In the next two sections, we describe the cDSP for the foam liner and the composite shell.

2.3.2.1 The compromise Decision Support Problem and Concept Exploration Framework for the Foam Liner

In Step 2 of our method, we use CEF processors A, B1, B2, C, D, E, and F to find satisficing solutions for the foam liner that achieve the system-level goals as close as possible. We show the CEF used in Steps 2 and 3 for the foam liner and composite shell analysis below in Figure 2.11.

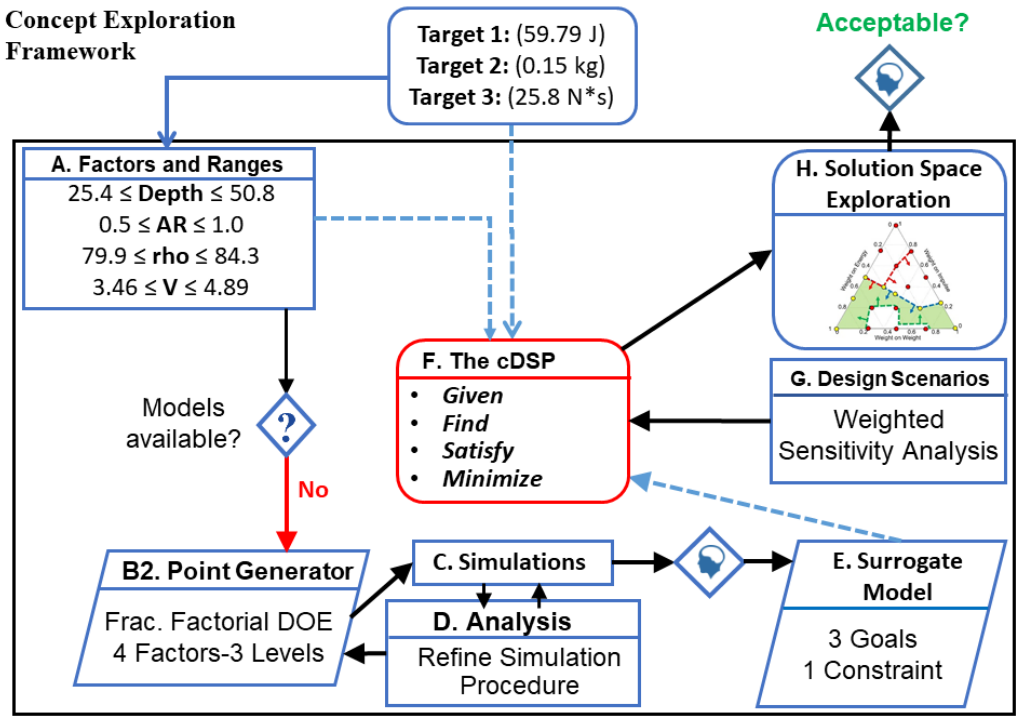

Figure 2.11 The Concept Exploration Framework (CEF) for the foam liner.

Targets 1, 2, and 3 correspond to our goals for internal energy (59.79 J), weight (0.15 kg), and impulse (25.8 N*s). We communicate the targets directly into the cDSP (Processor F). In Processor A, we list and communicate the foam depth, AR, density, and impact velocity variables and their respective ranges to the cDSP. We do not have math

models available for Processor B1, therefore we leave it out of the CEF formulation. As a result, we used processor B2, C, D, and E to create a set of metamodels from a DOE that describe the system-level goals and constraints in terms of the design variables (factors). Each of the four factors have lower, middle, and upper bounds (see Table 2.5). A three-level, four factor (3^4) full factorial DOE would require 81 simulations; however, to reduce the computational costs, we chose a fractional factorial DOE (3^{4-1}) that requires only 27 simulations. We show the 3^{4-1} DOE for the foam liner in Table 2.6 on the next page.

Table 2.6 Fractional factorial (3^{4-1}) Design of Experiments (DOE) for the foam liner.

Exp.	Depth (mm)	Area Ratio (AR)	Density (kg/m^3)	Velocity (m/s)
1	25.4	0.5	79.90	3.458
2	38.1	0.5	82.80	3.458
3	50.8	0.5	84.30	3.458
4	38.1	0.5	79.90	4.236
5	50.8	0.5	82.80	4.236
6	25.4	0.5	84.30	4.236
7	50.8	0.5	79.90	4.89
8	25.4	0.5	82.80	4.89
9	38.1	0.5	84.30	4.89
10	38.1	0.75	79.90	3.458
11	50.8	0.75	82.80	3.458
12	25.4	0.75	84.30	3.458
13	50.8	0.75	79.90	4.236
14	25.4	0.75	82.80	4.236
15	38.1	0.75	84.30	4.236
16	25.4	0.75	79.90	4.89
17	38.1	0.75	82.80	4.89
18	50.8	0.75	84.30	4.89
19	50.8	1	79.90	3.458
20	25.4	1	82.80	3.458
21	38.1	1	84.30	3.458
22	25.4	1	79.90	4.236
23	38.1	1	82.80	4.236
24	50.8	1	84.30	4.236
25	38.1	1	79.90	4.89
26	50.8	1	82.80	4.89
27	25.4	1	84.30	4.89

We used SolidWorks (Dassault Systems, Waltham, MA) to model the 27 DOE geometries and then imported the files into Abaqus Explicit CAE (Dassault Systems, Waltham, MA) for analysis. More information regarding the FEA can be found in Section 2.3.3. We used the response from the 27 DOE experiments to created four first-order polynomial response surface metamodels (response models). One for the three

system-level goals, and one to describe compression to use as a constraint. The four polynomial response models used in Step 2 are listed below.

Internal energy (IE) as a function of depth (D), AR, density (rho), and velocity (V).

$$IE(\mathrm{D}, \mathrm{AR}, \mathrm{rho}, \mathrm{V}) = -68.08173 + 178.7402 * \mathrm{D} + 4.544444 * \mathrm{AR} + 0.3706196 * \mathrm{rho} + 14.87528 * \mathrm{V} \quad (2.14)$$

Weight (Wt) as a function of depth (D), AR, and density (rho).

$$Wt(\mathrm{D}, \mathrm{AR}, \mathrm{rho}) = 0.028208 + 1.1566 * \mathrm{D} + 0.062556 * \mathrm{AR} + 0.000723 * \mathrm{rho} \quad (2.15)$$

Impulse (Imp) as a function of depth (D), AR, density (rho), and velocity (V).

$$Imp(\mathrm{D}, \mathrm{AR}, \mathrm{rho}, \mathrm{V}) = 5.15542 - 28.8714 * \mathrm{D} - 2.86444 * \mathrm{AR} - 0.0910578 * \mathrm{rho} + 9.65291 * \mathrm{V} \quad (2.16)$$

Compression (C) as a function of depth (D), AR, density (rho), and velocity (V).

$$C(\mathrm{D}, \mathrm{AR}, \mathrm{rho}, \mathrm{V}) = 0.15383 + 0.3535 * \mathrm{D} - 0.011584 * \mathrm{AR} - 0.0019516 * \mathrm{rho} + 0.0059301 * \mathrm{V} \quad (2.17)$$

We did not find much variation in the "goodness of fit" parameters between first, second, third, and fourth order response models. Therefore, we selected the first order models because they are much easier to formulate into the cDSP and should still provide a reasonably accurate result. The two "goodness of fit" parameters used were the Coefficient of Variation of the Mean Absolute Error (CVMAE) and R^2. We show the "goodness of fit" details for the four response models in Table 2.7 below.

Table 2.7 Goodness of fit details for the foam liner polynomial response models.

Response Model	**Internal Energy**	**Weight**	**Impulse**	**Compression**
Order	1	1	1	1
CVMAE	0.0725	0.0116	0.0475	0.0909
R^2	0.9283	0.9867	0.9249	0.9183

All design information regarding the factors and ranges from CEF processor A, and the metamodels created with processors B2, C, D, and E are fed into processor F to formulate the cDSP. We show the formal Step 2 cDSP including the four key *Given*, *Find*, *Satisfy*, *Minimize* sections below (Recall the problem description in Section 2.3.1).

Given:
(4) The system-level performance goals identified for our helmet region
- Maximize internal energy (IE)
- Minimize system weight (Wt)
- Minimize impulse (Imp)
- Minimize compression (comp)
- Achieve target energy dissipation (100%)
- Target value for internal energy, IE = 59.79 J
- Target value for system weight, Wt = 0.15 kg
- Target value for impulse = 25.78 N*s
- Maximum compression, C = D-12.7 mm

(5) The foam liner polynomial response models
- Internal energy (IE), see Equation 1
- Weight (Wt), see Equation 2
- Impulse (Imp), see Equation 3
- Compression (Comp), see Equation 4

(6) Variability in system variables
We provide the system variables in the *Find* and *Satisfy* sections.

Find:
System Variables
X_1, foam depth (D) – 25.4 to 50.8 mm
X_2, Area Ratio (AR) – 0.5 to 1.0
X_3, foam density (rho) – 79.9 to 84.3 kg/m^3
X_4, impact velocity (V) – 3.46 to 4.89 m/s

Satisfy:

System Constraints

- Minimum Internal Energy Constraint

$$IE \geq 30\ J \tag{2.18}$$

- Maximum Weight Constraint

$$Wt \leq 0.213\ kg \tag{2.19}$$

- Maximum Impulse Constraint

$$Imp \leq 45.82\ N * s \tag{2.20}$$

- Maximum Compression Constraint

$$D - Comp \geq 12.7\ mm \tag{2.21}$$

System Goals

Goal 1:

- Maximize Internal Energy

$$\frac{IE(X_i)}{IE_{Target}} + d_1^- - d_1^+ = 1 \tag{2.22}$$

Goal 2:

- Minimize System Weight

$$\frac{Wt_{Target}}{Wt(X_i)} - d_2^- + d_2^+ = 1 \tag{2.23}$$

Goal 3:

- Minimize Impulse

$$\frac{Imp_{Target}}{Imp(X_i)} - d_3^- + d_3^+ = 1 \tag{2.24}$$

V*ariable Bounds*

X_1 – 25.4 to 50.8 mm

X_2 – 0.5 to 1.0

X_3 – 79.9 to 84.3 kg/m^3

X_4 – 3.46 to 4.89 m/s

Bounds on deviation variables

$$d_i^-, d_i^+ \geq 0\ and\ d_i^- * d_i^+ = 0, i = 1,2,3 \tag{2.25}$$

Minimize:

We minimize the deviation function.

$$Z = \sum_{i=1}^{3} W_i(d_i^- + d_i^+); \sum_{i=1}^{3} W_i = 1 \tag{2.26}$$

We formulate the cDSP (shown above) in processor F, and then run it 19 times according to a weight sensitivity analysis in processor G to obtain 19 design points. In the last CEF processor H we plot the design points with a ternary plot and then explore the solution space to find satisficing solutions for each of our design goals. Finally, we make design decisions and pass the hard design information back to formulate the cDSP in Step

3 with respect to the new information and modified design goals. More information regarding the weight sensitivity analysis (processor G) and solution space exploration (processor H) will be discussed in Section 2.3.4. In the next section, we describe the cDSP for the Step 3 composite shell.

2.3.2.2 The compromise Decision Support Problem and Concept Exploration Framework for the Composite Shell

Step 3 of our method is very similar to Step 2; however, we set the targets for the shell using the modified requirements and goals passed back from the foam liner analysis (Step 2). Because we use the foam geometry from the Step 2 design decisions, we only need to vary the shell design variables in this step. Additionally, we selected an impact velocity in Step 2 that we hold constant in this analysis.

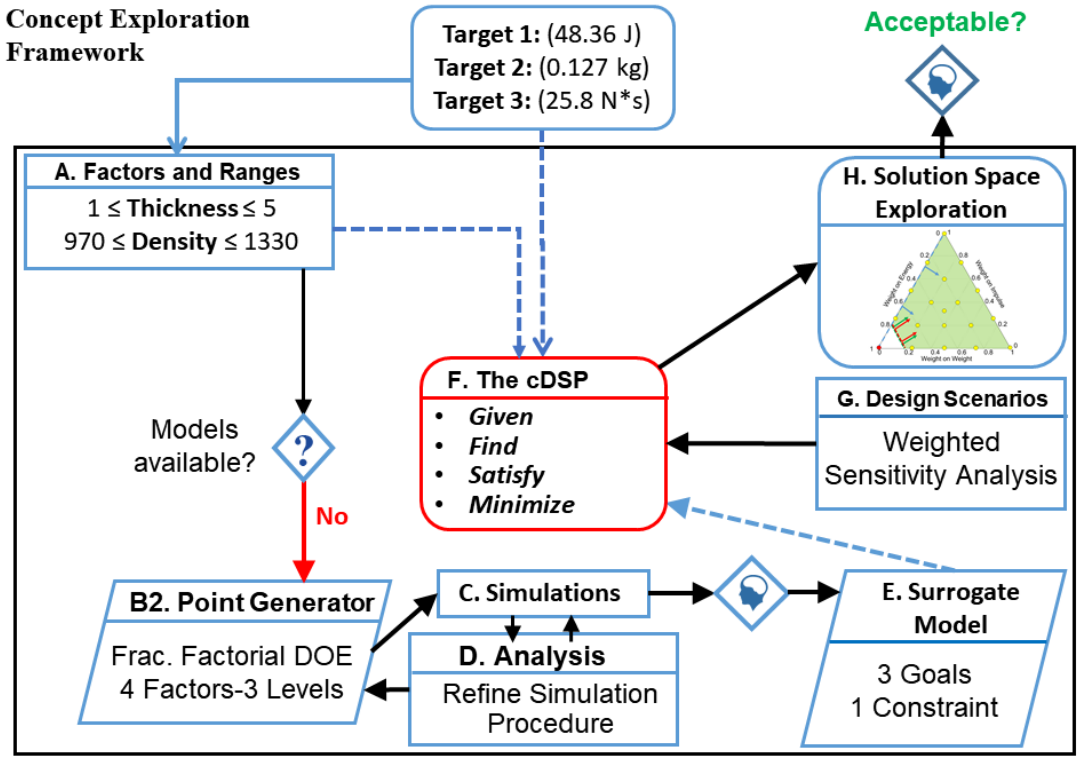

Figure 2.12 The Concept Exploration Framework (CEF) for the composite shell.

The three target values listed in Figure 2.12 above correspond to the adjusted targets from Step 2. We identify only two factors for the shell, namely, thickness and composite density, which we determine from the volume fraction of E-glass fiber. Both factors had three levels (3^2), which is only 9 experiments, therefore time we used a full factorial DOE. We show the (3^2) full-factorial DOE in Table 2.8 below.

Table 2.8 Full factorial (3^2) Design of Experiments (DOE) for the composite shell.

Exp.	Thickness (mm)	Density (kg/m^3)
1	1	970
2	1	1120
3	1	1330
4	3	970
5	3	1120
6	3	1330
7	5	970
8	5	1120
9	5	1330

We used DOE run number 24 from Step 2 as our baseline mesh for this analysis. To model the 9 DOE composite shell variations, we simply converted the composite shell mesh from 3D continuum elements to shell elements in Abaqus Explicit CAE (Dassault Systems, Waltham, MA) and then we assigned shell thickness values depending on the experiment. More information regarding the FEA can be found in Section 2.3.3. We used the response from the 9 DOE experiments to re-create the four polynomial response surface metamodels (response models) from Step 2. The four polynomial response models used in Step 3 are listed below.

Internal energy (IE) as a function of thickness (t) and density (rho).

$$\mathrm{IE}(\mathrm{t},\mathrm{rho}) = 0.0120015318 * \mathrm{rho} + 1760.927676 * \mathrm{t} - 0.3183868502 * \mathrm{t} * \mathrm{rho} + 38.14990639 - 208262.5 * (\mathrm{t}\text{^}2) - (4.43324515 * (10\text{^}(-06)) * (\mathrm{rho}\text{^}2)) \quad (2.27)$$

Weight (Wt) as a function of thickness (t) and density (rho).

$$\mathrm{Wt(t,rho)} = 3.2817108 * (10\text{^}(-06)) * \mathrm{rho} + 10.02042 * \mathrm{t} + 0.033070678 * \mathrm{t} * \mathrm{rho} + 0.083487294 - 1670.0701 * (\mathrm{t\text{^}2}) + (4.9352724 * (10\text{^} - 22) * (\mathrm{rho\text{^}2})) \quad (2.28)$$

Impulse (Imp) as a function of thickness (t) and density (rho).

$$\mathrm{Imp(t,rho)} = -0.003511421371 * \mathrm{rho} + 1245.756881 * \mathrm{t} - 0.04013761468 * \mathrm{t} * \mathrm{rho} + 42.14854726 - 151250 * \mathrm{t} ** 2 + (1.631393298 * (10\text{^}(-06)) * (\mathrm{rho\text{^}2})) \quad (2.29)$$

Compression (C) as a function of thickness (t) and density (rho).

$$\mathrm{C(t,rho)} = 0.032028 - 1.2323 * \mathrm{t} - (5.414 * (10 ** (-06)) * \mathrm{rho}) \quad (2.30)$$

We found the "goodness of fit" parameters dropped from the previous analysis, likely because there were fewer design points (9 instead of 27). Therefore, we selected the best alternative among the first, second, third, and fourth order response models. The two "goodness of fit" parameters used were the CVMAE and R^2. We show the "goodness of fit" details for the four response models in Table 2.9 below.

Table 2.9 Goodness of fit details for composite shell polynomial response models.

Response	**Internal Energy**	**Weight**	**Impulse**	**Compression**
Order	2	2	2	1
CVMAE	0.0232	0.0063	0.0067	0.0176
R^2	0.6269	1.0	0.9704	0.9820

Just as in Step 2, all design information collected through CEF processors A, B2, C, D, and E are fed into processor F to formulate the cDSP. We show the formal Step 3

cDSP including the four *Given, Find, Satisfy, Minimize* sections below (Recall the problem description in Section 2.3.1).

Given:

(7) The adjusted performance goals identified for our shell

- Maintain internal energy (IE)
- Minimize system weight (Wt)
- Minimize impulse (Imp)
- Minimize compression (comp)
- Achieve target energy dissipation
- Target value for internal energy, IE = 48.36 J
- Target value for system weight, Wt = 0.127 kg
- Target value for impulse = 41.32 N*s
- Maximum compression, C = D-12.7 mm

(8) The composite shell polynomial response models

- Internal energy (IE), see Equation 14
- Weight (Wt), see Equation 15
- Impulse (Imp), see Equation 16
- Compression (Comp), see Equation 17

(9) Variability in system variables

We provide the system variables in the *Find* and *Satisfy* sections.

Find:

System Variables

X_1, shell thickness (t) – 1 to 5 mm

X_2, density (rho) – 970 to 1330 kg/m^3

Satisfy:

System Constraints

- Minimum Internal Energy Constraint

$$IE \geq 46.3\ J \tag{2.31}$$

- Maximum Weight Constraint

$$Wt \leq 0.213\ kg \tag{2.32}$$

- Maximum Impulse Constraint

$$Imp \leq 41.8\ N * s \tag{2.33}$$

- Maximum Compression Constraint

$$D - Comp \geq 12.7\ mm \tag{2.34}$$

System Goals

Goal 1:

- Maximize Internal Energy

$$\frac{IE(X_i)}{IE_{Target}} + d_4^- - d_4^+ = 1 \quad (2.35)$$

Goal 2:

- Minimize System Weight

$$\frac{Wt_{Target}}{Wt(X_i)} - d_5^- + d_5^+ = 1 \quad (2.36)$$

Goal 3:

- Minimize Impulse

$$\frac{Imp_{Target}}{Imp(X_i)} - d_6^- + d_6^+ = 1 \quad (2.37)$$

V*ariable Bounds*

X_1 – 1 to 5 mm

X_2 – 970 to 1330 kg/m^3

Bounds on deviation variables

$$d_i^-, d_i^+ \geq 0 \text{ and } d_i^- * d_i^+ = 0, i = 1,2,3 \quad (2.38)$$

Minimize:

We minimize the deviation function.

$$Z = \sum_{i=1}^{3} W_i(d_i^- + d_i^+); \sum_{i=1}^{3} W_i = 1 \quad (2.39)$$

We formulate the cDSP (shown above) in processor F, and then run it 19 times according to a weight sensitivity analysis in processor G to obtain 19 design points. In the last CEF processor H we plot the design points with a ternary plot and then explore the solution space to find satisficing solutions for each of our design goals. Finally, we make design decisions verify our final results with FEA. In the next section, we review the FEA models used to develop the metamodels and verify our design results.

2.3.3 Finite Element Analysis for the Foam Liner and Composite Shell

In this section we describe the FEA models used to develop the four metamodels for Step 2, the four metamodels for Step 3, and verify both of the design results in Step 4. We created 27 FE meshes for Step 2 (one for each DOE runs), 3 meshes for Step 3 (1 mesh per three DOE runs), where the two meshes for Step 4 (verification) were taken

from the previous analysis, making 30 different meshes and 38 simulations total. Each mesh includes a shell and a foam liner that consists of 4 foam blocks and a "plug" in the center. The stress wave damper can replace the "plug" in future work. First, we modeled the baseline geometry using the top region of the actual full-scale prototype helmet in SolidWorks. We show an example of the of the top region geometry in Figure 2.13 below.

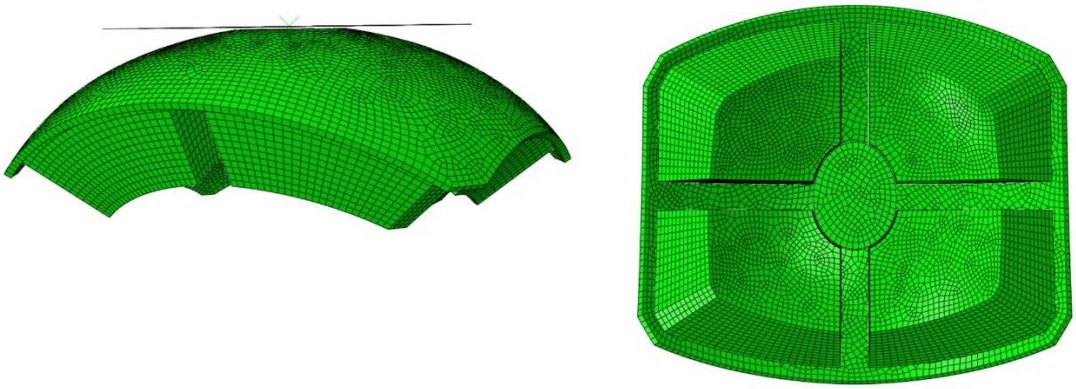

Figure 2.13 Example top helmet region geometry used for Finite Element Analysis (FEA) showing the shell-side (left), and the foam liner side (right).

In Step 2, we use the baseline 3 mm shell thickness and create the 27 foam liner geometries according to the DOE specifications in Table 2.6. We used the geometries from DOE runs 19-27 as our baseline design and then vary the gap distance between the foam blocks to achieve the appropriate Area Ratio for the other geometries. We did this because the Area Ratio does not change linearly as the thickness changes. The design decision from Step 2 closely matched one of the 27 models, therefore in Step 3 we held the selected foam liner geometry but changed the shell thickness depending on the DOE specifications. The geometry specifications for both Step 4 verification analysis were close enough to previous geometries that we reused meshes and only altered the material properties and boundary conditions.

For this analysis, we modeled 7 different materials, including 3 shell options, 3 foam options, and 1 additional shell option for the final design verification. We select three densities of SunMate brand foam (viscoelastic slow recovery, open-cell polyurethane foam) available for purchase: Medium (79.9 kg/m^3), Medium-Firm (82.8 kg/m^3), and Firm (84.3 kg/m^3). We used low rate (0.1/s) and high rate (600/s) compression test data collected by Rush et al. [48] to model the foam materials using the elastic, low-density foam model available in Abaqus Explicit CAE. The baseline composite shell material is an injection moldable polypropylene (PP) matrix with short, Chemically Coupled (CC) E-glass fibers manufactured by RTP Co.. In step 2, we selected three options from their list of RTP 100 series (PP with short E-glass CC fibers) that ranged from 10 to 50% E-glass. We modeled RTP 101 CC (10% E-glass), 105 CC (30% E-glass) and 109 CC (50% E-glass) as linear elastic-plastic materials using uniaxial tension test data provided by the manufacturer. The shell material decision made in Step 3 most closely resembled the RTP 103 CC (20% E-glass) material; therefore, we created a fourth shell material to complete the Step 4 verification analysis. We conducted a single element FEA to verify each material by comparing the stress-strain behavior to their respective source. We list the materials used in our analysis in Table 2.10 below.

Table 2.10 Material properties for the 3 foam densities and 4 shell materials used in this analysis.

Material	Material Model	Density (tonne/mm^3)	Elastic Modulus (MPa)	Poisson's Ratio
Medium	Low Density Foam	$7.99*10^{-11}$	N/A	N/A
Medium-Firm	Low Density Foam	$8.28*10^{-11}$	N/A	N/A
Firm	Low Density Foam	$8.43*10^{-11}$	N/A	N/A
RTP 101	Elastic-Plastic	$9.7*10^{-10}$	3103	0.281
RTP 103	Elastic-Plastic	$1.03*10^{-9}$	4482	0.212
RTP 105	Elastic-Plastic	$1.12*10^{-9}$	6206	0.25
RTP 109	Elastic-Plastic	$1.33*10^{-9}$	11722	0.334

We conducted a mesh refinement in another study with a similar geometry that consist of a curved 3 mm shell and a foam liner with similar dimensions. We conducted an h-refinement and p-refinement where we increased the number of elements, and also increased the order of elements, respectively. For both components, the linear elements in the h-refinement had 8 nodes and 1 integration point (C3D8R) where the quadratic elements in the p-refinement had 20 nodes and 8 integration points (C3D20R). We partitioned the shell into 4 quadrants, and the rest of the components were left in their original configuration. For each analysis, we verified the mesh did not have errors and all aspect ratios less than 5, with the majority less than 3. The refinement study was concluded after 14 job submissions, 7 refinements for the h-refinement and 7 refinements for the p-refinement. Therefore, each component had 14 total alternative mesh scenarios. From the results, we determined linear C3D8R elements were acceptable for both parts

and a global seed size of 1.5 for the shell and 3 for the foam liner. In Step 3, we converted the shell component from C3D8R elements S4R shell elements and verified our results were not influenced by the element type conversion. Table 2.11 below lists the average mesh details for the Step 2, 3, and 4 analysis.

Table 2.11 Finite element average mesh details for the Step 2, 3, and 4 analysis.

	# nodes	C3D8R elements	S4R elements	CPU time
Step 2	52253	41071	N/A	0:58:83
Step 3	64286	51833	5387	1:45:30
Step 4	67101	54527	5387	2:41:25

In the next section, we describe the weight sensitivity analysis, solution space exploration, and design decisions made for Step 2 and 3.

2.3.4 Integrated Solution Space Exploration of the Foam Liner and Composite Shell

Herein, we describe the integrated solution space exploration of the foam liner with respect to the system-level goals and the composite shell with respect to the modified requirements and goals. Both cDSP's for the foam liner and composite shell were exercised 19 times to generate 19 sets of design alternatives. As we discussed before, the weights range from 0 to 1 where a value of 1 represents the highest preference, and a value of 0 represents no preference. Scenarios 1-3 represent a maximum weight assignment to find design solutions that satisfy the design requirements and achieves a goal as close as possible with no preference on the other goals. Using the foam liner cDSP as an example, with Scenario 1, we find a solution for the foam liner depth, AR, density, and impact velocity variables that lie within the specified constraints and achieves the internal energy target as close as possible with no preference to weight

or impulse. Scenarios 4-6 split the preference between two goals equally, while giving no preference to the third goal. Scenarios 7-12 give a higher preference to one goal, a low preference to another goal, and no preference to the last goal. Scenario 13 represents an equal preference split among the three goals. Scenarios 14-19 distribute the preference among the three goals in different amounts. Exercising the cDSP for all 19 weight assignments gives the minimum number of design alternatives needed to span the ternary design space. In our analysis, our objectives were to maximize internal energy, minimize weight, and minimize impulse. Therefore, we desire a normalized solution of 1 for the internal energy goal and 0 for the weight and impulse goals because they would represent the maximum and minimum values, respectively. After creating the 19 design points, we visualize the solution space by assigning color values to the normalized solutions. Then, we can draw boundaries on each plot based on our preference. To visualize all three goals we generate four ternary plots, one to show the goal attainment for each of the three goals, and the fourth reveals the overlapping, or satisficing, region. In the following section, we describe the solution space exploration for the foam liner and the composite shell cDSPs and then explain the tradeoffs necessary to find a satisficing design.

2.3.4.1 Solution Space Exploration and Tradeoff Analysis of the Foam Liner to Achieve the System-Level Goals

The requirement for the designer in Step 2 is to find values for the foam liner design variables that achieve the system-level goals as close as possible. For the internal energy goal in the liner cDSP, we are interested in dissipating the maximum impact energy possible. Assuming the worst-case scenario from the impact velocities listed earlier, we set the target for the internal energy goal at 59.78 J, which would mean a

100% dissipation, and assign a constraint of 30 J. In other words, we desire 100% dissipation, but we require at least 50% dissipation in the worst-case impact scenario. For the weight Goal 2, we are interested in minimizing the total weight of the region, the smaller the better. We set the target weight equivalent to the minimum possible weight, from the DOE, that corresponds to approximately 0.15 kg. Likewise, we constrained the system to a weight equivalent to the maximum weight from the DOE that is approximately 0.213 kg. In other words, we desire the lightest region, with a maximum weight of 0.213 kg. For the impulse Goal 3, we are interested in minimizing the impulse experienced by the head. We calculated the impulse by taking the time integral of the reaction force at the pinned nodes on the foam liner. Lower impulse values represent a higher stress wave mitigation, lower force magnitudes, or a shorter impact duration. Like the weight constraints, we set the target impulse value as the minimum value achieved from the DOE, that is 25.78 N*s and constrained the maximum impulse to 45.82 N*s. The cDSP and design variable constraints were listed in Section 2.3.2.

We exercised the cDSP 19 times and generated 19 sets of solutions for the foam liner depth, area ratio (AR), foam density, and impact velocity that all fall within our design constraints. We plug the design variable values into the polynomial response models to find values for each of our design goals. We created three sets of normalized goal values (one for each goal) using the following equation,

$$\frac{Y_i - min}{max - min} \tag{2.40}$$

where Y_i is the goal value of point i from 1 to 19, min is the minimum value, and max is the maximum value in the range of design points. We used the three sets of normalized goal values to create the three ternary plots shown in Figure 2.14 below.

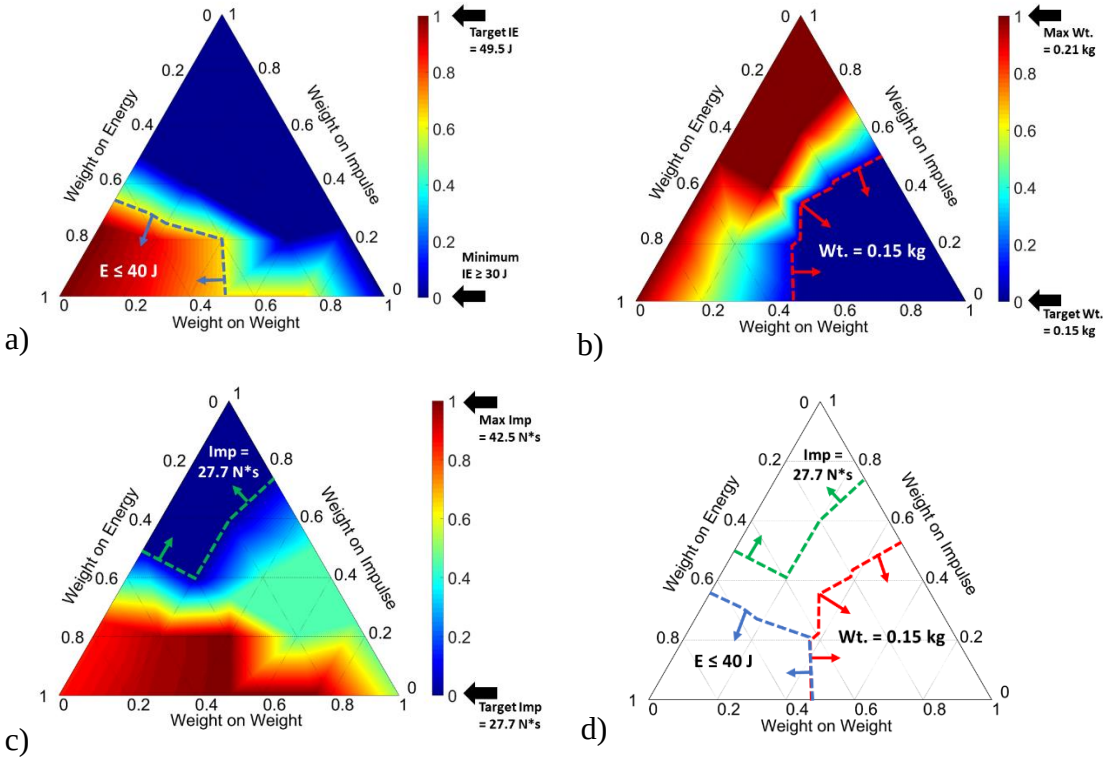

Figure 2.14 Ternary plots showing the goal attainment for a) internal energy (Goal 1), b) weight (Goal 2), c) impulse (Goal 3), and d) overlapping.

Figure 2.14-a shows the liner cDSP results when we normalize the internal energy (Goal 1) values. The target of 59.78 J (100% dissipation) was unobtainable, however the maximum internal energy achievable under the design constraints was 49.5 J. Therefore, 49.5 J becomes our target, normalized value of 1 and appears dark red on the plot. We set a preference boundary, shown by the dark blue dashed line, to limit the preferred design space to 40 J internal energy or higher. Figure 2.14-b shows the liner cDSP results when we normalized the weight (Goal 2) values. The target weight was 0.15 kg and because it should be the minimum result, the normalized value is 0 and appears as dark blue. There is not much variation in the weight goal results. Therefore, we set a preference boundary, shown by the bright red dashed line, to include all design points that achieved our target

weight of 0.15 kg. Figure 2.14-c shows the normalized impulse (Goal 3) values where the target impulse value of 25.78 N*s appears as dark blue. We set a preference boundary, shown by the lime green dashed line, to include all results with 27.7 N*s or lower. To set the preference boundaries, we are essentially bounding the solution space to the results that most closely achieve our goals. One can observe the conflicting nature of these three goals from the preferred color concentrations located in opposite corners of the ternary plot. Figure 2.14-d shows the preferred design regions for each goal overlapped onto one ternary plot. Ideally, there would be an overlapping region that contains all the satisficing solutions for the three goals. In other words, to obtain the optimal solution with respect to one goal, we must sacrifice the performance of another. To find a satisficing region, we must make a compromise and relax the preferred boundaries for each goal until we find a satisficing region. We decided to relax our desired solution for internal energy to include all design points that have internal energies greater than 30 J. Likewise, we relax the boundaries for goals 2 and 3 to include design points with values less than 0.21 kg and impulse values less than 41 N*s. We show the adjusted solution space including the satisficing region (green) and satisficing design points in Figure 2.15 below.

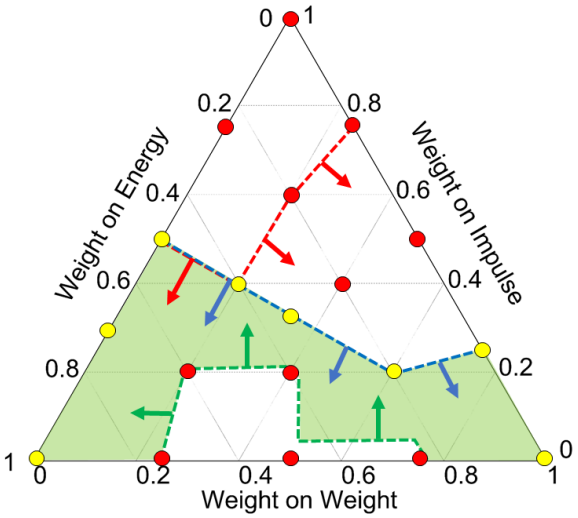

Figure 2.15 Satisficing solution region for the foam liner showing 8 satisficing design points (Yellow) and 11 non-satisficing points (Red).

Figure 2.15 above shows the relaxed preference boundaries for Goal 1, Goal 2, and Goal 3 as blue, red, and greed dashed lines, respectively. The arrows indicate the direction of preference, each dot represents a design point where the yellow points are satisficing, and the red points are not. The green region, or satisficing region, contains only 8 satisficing design points. This means all design points within the green region satisfy all three system-level requirements while attaining the goals as close as possible. It is now up to the human designer to make a decision from the available satisficing design alternatives. In the early stages of our design process, it is somewhat difficult to determine which alternative is most attractive. Therefore, to assist in decision-making during the conceptual stages, we constructed a simple Multi-Criteria Decision Making (MCDM) routine to rank the satisficing design alternatives from 1 to 8 using a prescribed set of weight factors. We started by scaling the actual goal data for the 8 designs with the Ideal Value (IV) scaling method to normalize the set of goal data. Unlike the ternary plot normalization, the IV scaling takes into consideration the goal's objective and scales

from 0 to 1, where a value of 1 represents the best alternative with respect to the objective. At this point in the design process, we did not yet know the best weight factor distribution. However, from the FEA results, we observed the foam liner had a major influence on the internal energy, therefore we assign the highest weight to Goal 1 and then equally distribute the remainder among the other two goals. Then, we multiply the set of ideal values by their respective weight factors, sum the products, and then rank the results where the highest result denotes the best alternative. We display the results from the MCDM raking analysis in Table 2.12 below.

Table 2.12 Multi Criteria Decision Making (MCDM) matrix and rank results for satisficing foam liner design points.

		Goal 1	**Goal 2**	**Goal 3**		
	Weight	**0.50**	**0.25**	**0.25**	**Total**	**Rank**
	Scenario					
Feasible Scenarios	1	1.000	0.712	0.686	0.850	1
	2	0.604	1.000	0.784	0.748	6
	5	0.606	0.712	1.000	0.731	7
	9	1.000	0.712	0.686	0.850	2
	11	0.607	0.999	0.808	0.755	5
	13	0.607	0.999	0.808	0.755	4
	15	0.606	0.712	1.000	0.731	8
	19	0.607	0.999	0.808	0.755	3

After reviewing the MCDM results, we select the number 1 ranking scenario, Scenario 1, from the list of satisficing solutions. The actual design variables for scenario 1, calculated from the cDSP, were a depth of 50.8 mm, an AR of 0.99, a density of 84.3 kg, and an impact velocity of 4.89 m/s. Using our response surface equations for the foam liner (1-4), we calculate an internal energy value of 49.52 J, a total system weight of 0.21 kg, and an impulse value of 40.35 N*s. In other words, this design would be able to

dissipate approximately 83% of the impact force ((59.78 J - 49.52 J)/59.78 J, where 59.78 J was the 100% design goal) from a 4 ft. NOCSAE standard drop test.

The MCDM ranking routine was only applied for the feasible results, however, if we were to perform this routine including all 19 design points, without regard for our preference boundaries, we would find the best alternative was Scenario 10. Scenario 10 had an internal energy value of 47.24 J, a weight of 0.18 kg, and an impulse of 41.78 N*s. While this scenario may have a high internal energy value, and a low weight, the solution point for impulse lies outside the relaxed preference boundary. Additionally, scenario 10 had a maximum compression of 30.5 mm, which is close to our maximum compression constraint. We made the weight tradeoff and selected design point 1 over design point 10 because point 1 satisfies all the goals and in the next analysis we can design the shell component with a higher priority on lowering the system weight.

Finally, we ran a FE verification analysis with the Scenario 1 design variables. The design variables are very close to one of the DOE meshes, so we reused mesh 24 and only changed the input velocity to 4.89 m/s. We show the FEA design variable input parameters and goal value results for comparison to the cDSP calculation in Table 2.13 below.

Table 2.13 Step 2, scenario 1 compromise Decision Support Problem (cDSP) results compared to Finite Element Analysis (FEA) results.

Parameter	cDSP result	FEA result	error
Depth (m)	0.05079	0.0508	0.02%
AR	0.999	1	0.10%
Density (kg/m^3)	84.299	84.3	0.00%
Velocity (m/s)	4.8897	4.89	0.01%
Internal Energy (J)	49.52	48.36	-2.34%
Weight (kg)	0.2104	0.2132	1.35%
Impulse (N*s)	40.35	41.80	3.58%
Compression (m)	0.0247	0.0220	-10.84%

We find good agreement between the FEA results and the cDSP results. We observe the internal energy value decreases by 2.34%, the total weight increases by 1.35%, and the impulse increases by 3.58%. While these are not desirable shifts in performance, they are still acceptable and fall within a reasonable uncertainty band. The final FEA results show our helmet region can dissipate approximately 81% of the maximum input kinetic energy, weighs approximately 0.213 kg, and has a high impulse value of 41.8 N*s. We can now move on to Step 3 and pass this design information, along with modified goals back to design the composite shell.

2.3.4.2 Solution Space Exploration of the Composite Shell to Achieve the Modified System Goals

The design decisions made in the solution space exploration for the foam liner (Step 2) frame the problem for the composite shell design (Step 3). Our requirement is to find satisficing solutions for the composite shell thickness and density that maintain the internal energy goal from Step 2 while further achieving the weight and impulse goals 2 and 3. The composite shell shares the same set of system-level goals with the foam liner;

however, we adjust the goal targets and constraints according the results from Step 2. We set the new target for the internal energy goal at 48.36 J, and constrain the minimum drop in internal energy to 5%, or a minimum of 46.3 J. For the weight and impulse goals, we desire the minimum possible value while constraining the maximum value to the results from Step 2. This means our new weight target is 0.127 kg with a maximum constraint of 0.213 kg and the new impulse target is 41.32 N*s with a maximum of 41.80 N*s. We use the same process from Step 2, to construct the cDSP, and run 19 weight sensitivity iterations, and then plot the solution spaces. In Figure 2.16 we show the three ternary plots for our three goals and the overlapping, satisficing ternary plot.

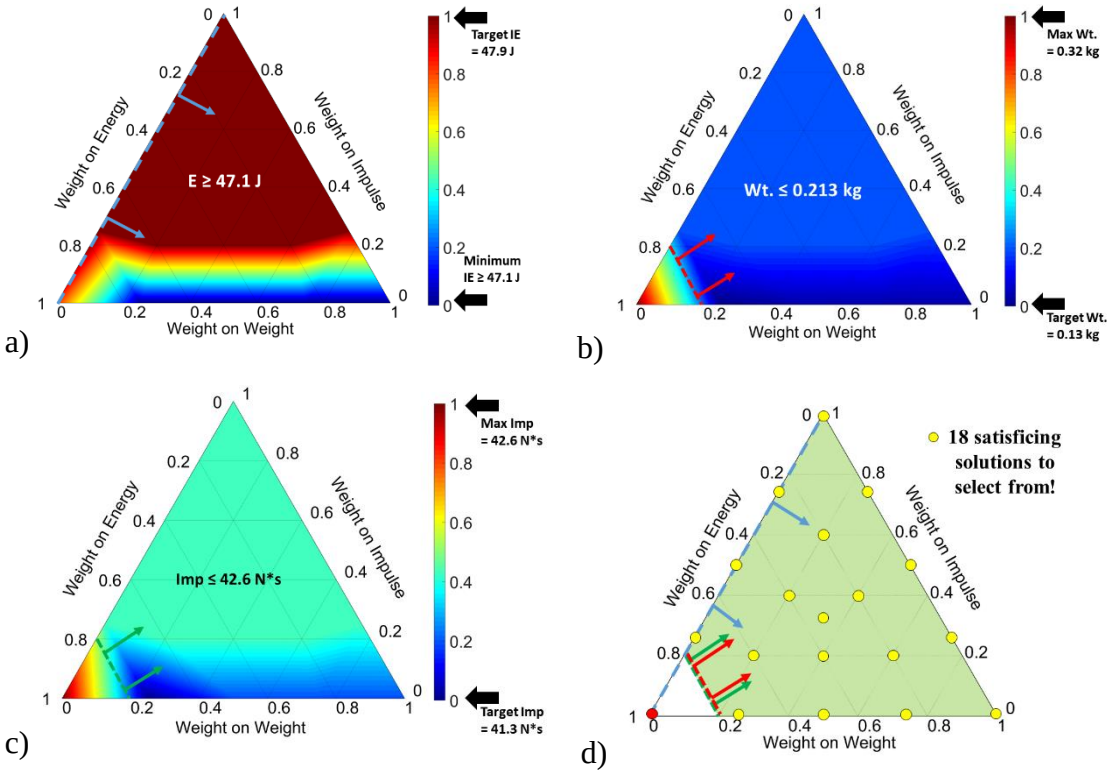

Figure 2.16 Ternary plots showing the goal attainment for a) internal energy (Goal 1), b) weight (Goal 2), c) impulse (Goal 3), and d) overlapping.

All design points satisfy our internal energy requirements. We do not find it necessary to make any preference boundary adjustments. When we combine the plots, we find almost all design points are feasible, leaving only one point outside our requirements. It is once again up to the designer to choose between the 18 satisficing design alternatives. This time, we expand our MCDM routine to rank 18 alternatives where we assign equal weight factors of 0.5 to the weight and impulse goals and no weight on internal energy. We list the top three results, with their associated goal and design variable values below in Table 2.14.

Table 2.14 Top 3 Multi Criteria Decision Making (MCDM) ranked scenarios, goal values, and design variable values.

Run (rank)	Goal 1 IE (J)	Goal 2 Wt. (kg)	Goal 3 Imp (N*s)	Thickness (mm)	Density (kg/m^3)
10 (1)	47.12	0.131	41.33	1.02	1061
4 (2)	47.12	0.137	41.56	1.26	970.12
7 (3)	47.12	0.137	41.56	1.26	970.12

We select the number 1 ranked satisficing scenario, Scenario 10, as our Step 3 composite shell design for verification in Step 4. Scenario 10 maintains the internal energy value from Step 2 within 5% (down from 49.52 J), shows a 37.6% reduction in system weight (down from 0.21 kg), and a 2.4% rise in impulse (up from 40.35 N*s). To verify this result, we reuse a FE mesh from the DOE simulations that has a shell thickness of 1 mm and change the material to match the suggested density value. We could construct our own composite from this specification, however, at this time we are limited to the composites available from RTP Co. We selected the RTP 103 CC (PP with 20% E-glass fiber) because the composite density is 1030 kg/m^3, which is only 2.95%

higher than the cDSP result. We show the FEA design variable input parameters and goal value results for comparison to the cDSP calculation in Table 2.15 below.

Table 2.15 Step 3, scenario 1 compromise Decision Support Problem (cDSP) results compared to Finite Element Analysis (FEA) results.

Parameter	cDSP result	FEA result	error
X1: thickness (t)	0.00102	0.0010	-1.56%
X2: density (rho)	1061.3	1030	-2.95%
Internal Energy (J)	47.12	48.30	2.49%
Weight (kg)	0.1311	0.1295	-1.21%
Impulse (N*s)	41.33	44.68	8.12%
Compression (m)	0.0250	0.0251	0.34%

When we compare the FEA verification result to the Step 3 cDSP results we see internal energy rise 2.49%, weight drop 1.21%, and impulse rise 8.12%. While the impulse value rise is outside the current design constraints, it is still below the system-level constraint of 45.82 N*s. Comparing the Step 3 FEA results in Table 2.15 to the Step 2 FEA results in Table 2.13, the internal energy value essentially remains constant (<1%) while the weight drops from 0.213 kg to 0.130 (39%). In other words, our final design would be able to dissipate approximately 81% of the impact force ((59.78 J - 48.3 J)/59.78 J, where 59.78 J was the 100% design goal) from a 4 ft. NOCSAE standard drop test while meeting our adjusted weight design goal within 2% ((0.130 kg - 0.127 kg)/0.127 kg, where 0.127 kg was the design goal).

2.4 Summary and Conclusions

In this chapter, we describe the elements of the Gero [57], Suh [58], Mistree et al. [59-61], and Nellippallil et al. [55, 67, 69-73] design process philosophies that form the foundation of our goal-oriented, inverse decision-based design method for helmet design.

Then we illustrated the efficacy of the method for multi-component product design in two ways. First, we exercised the CEF and cDSP constructs and solution space exploration with ternary plot tool to design a simplified section of the foam liner considering three conflicting goals. We use a flat representation of the helmet with only six foam liner pods in Section 2.2 so that we could exercise the method and constructs easily. This helped us to establish confidence in the method and constructs. We assumed we would be able to make changes to the components and reiterate with geometry from the actual helmet in the next exercise. In Section 2.3, we increased the complexity to design the top region of our prototype helmet and found satisficing solutions for the foam liner and the composite shell with respect to the same set of system-level goals. This helped us establish confidence that we could design at least two components within the same system boundary. The primary assumption here is that we will be able to reformulate the problem to include the additional bio-inspired components mentioned in Chapter 1. We also assume we will be able to design the other helmet regions that make up the complete assembly in parallel with respect to the same set of system level goals.

While we were not primarily interested in finding "good" helmet results, we were interested in how well our system was able to attain the selected target values. Overall, we designed the foam liner to dissipate 81% of the impact energy the helmet region would receive from a 4-foot standard NOCSAE drop test. Then, we found a solution for the composite shell that reduced the weight by 39% while maintaining the energy dissipation goals. With respect to the system-level goals, we were close to achieving our target value of 100% dissipation for Goal 1. At that stage in the design process, we did not have good results for Goals 2 and 3, but because we have a new set of design

variables for the shell, we reset the goal targets and found good achievement for Goal 2, but poor achievement for Goal 3. However, the framework is modular and we assume we can add a third or fourth component in a similar fashion to focus on achieving Goal 3. Therefore, demonstrating the design of at least two components was foundational to future work with additional components.

In this Chapter, we were able to demonstrate the following advantages of our selected method:

- Enabling a product designer to explore the design of multiple components within the same system boundary while retaining the ability to make modifications as the problem changes thereby managing the complexities to account for the emergent properties that cannot be predicted.
- For helmet design, the method allows us to define performance requirements for each component and connect their effects on the targeted system-level performance goals.
- Supports solution space exploration to find a compromise between satisficing solutions and costly iterations
- Supports simulation-based design
- A modular and generic method to allow us to reformulate the problem at will and then substitute components to design for other helmets in the same product family.
    - Modularity exists in the problem formulation (Step 1) as we just mentioned, but also in the analysis (Steps 2 and 3) where the

designer may iterate preferences and goals to find satisficing solutions.

Demonstrating the forward information flow and goal-oriented, inverse design of two components using linked cDSPs was foundational for future helmet design. In Chapter 3, we discuss the assumptions, method limitations, and future work regarding helmet design with our goal-oriented, inverse decision-based design method.

CHAPTER III

LIMITATIONS AND FUTURE WORK

3.1 Current Limitations

In this Chapter, we discuss the limitations in the problem formulation, the design analysis, and in the solution verification and then discuss our future work. To model the forward flow of information, we partition the helmet assembly into the individual components and arrange them in the order they receive impact energy. We limited the analysis to two simplified components, namely, the composite shell and the foam liner. Furthermore, we limit the geometry to one region of the helmet, as opposed to the entire helmet assembly. Individually designing the different helmet regions could be advantageous, but in the future, we need to design the regions with respect to the full-scale helmet assembly. We also need to include parameters such as the Thermoplastic Polyurethane (TPU) wrap and Velcro for the foam liner, or the paint on the composite shell to increase the accuracy of our formulation. Finally, in this thesis we simply demonstrate the linkage and design of two components and then leave the method open ended for the addition of extra components. In the future, we need to include every component subject to design, such as the bio-inspired concepts mentioned in Section 1.3. These additions would affect the formulation of the design problem, but the method should be modular enough to expand to incorporate the additional components. The overall system-level goals would remain the same, the soft information flowing into each

component would be different, and the specific targets we adjust for every component following Step 2 in our method (see Figure 2.1). The method requirement to order the components in a sequential way introduces another limitation in the design problem formulation. With respect to energy transfer, we have a logical way to order the components. However, with respect to goals such as system weight, there is no logical order. As we saw in Section 2.3, if we design one component with a higher priority on a goal such as internal energy, then the next component is responsible for picking up the slack on a goal such as system weight. Therefore, the design variables found for the second component are highly biased towards weight reduction that resulted in a poor result for the third goal (impulse). Expanding the method to include additional components may mitigate this effect, however in the future we need to modify the method to explore parallel formulations. We also need the method to remain generic for product design beyond helmets or situations where information is not easily passed between components in a logical forward process.

The design analysis for the current work was limited in three ways: the FEA, the cDSP, and solution space exploration with ternary plots. As we mentioned earlier, our method supports simulation-based design; therefore, we chose to collect the metamodel data from FEA simulations. These simulations are but approximations of reality and garner uncertainty in the pre-processing geometry, mesh, element type, material models, boundary conditions, calculations, etc. that results in uncertainty in the results. The metamodels are already approximations of the system response and carry their own uncertainty, not to mention the additional uncertainty brought in from the FEA. In the future, we can alleviate some of this uncertainty with more accurate FEA models, or

metamodels. However, the ultimate goal is to formulate our design problem to find solutions that are insensitive, or robust, against uncertainty, rather than attempting to eliminate it completely, which may be impossible. This design philosophy is called Robust Design. We discuss the Robust Design philosophy in greater detail in the next section. Because we only identified, not quantify, the sources of uncertainty in this thesis, we did not take full advantage of the cDSP. The cDSP was formulated by Bras et al. [65] to find satisficing solutions under uncertainty, or robust designs. We discuss the robust formulation of the cDSP in the next section. The cDSP can be an excellent tool for finding design variable values that satisfy a set of conflicting goals; however, with a fewer number of design variables, say 2 or 4, the results tend to congregate at the upper or lower variable bounds. For instance, if the foam depth design variable minimum and maximum were 25.4 and 50.8 mm, respectively, then almost all 19 results (from the weight sensitivity analysis) would either be 25.4 or 50.8 mm. This phenomenon might be avoided if we exercised more than the minimum (19) number of weight sensitivity iterations. This, or manually changing the design variable limits to force the program to find solutions in between the real constraints. Finally, the solution space exploration tool we selected, the ternary plots, limits our design formulation to three goals. In some cases, the designer may only be interested in one or two goals. In which case, more simplistic plots could show the relative goal attainments. However, in the case with more complex products, or multipurpose products, the designer may be interested in four or more system-level goals. For instance, in our future helmet design efforts, we will want to design for the current system-level goals, but also additional goals such as fatigue life or

the brain's response. In which case, we need a way to visualize the solution space and find satisficing solutions for four or more conflicting goals.

Our final limitation in this thesis was our method of verifying the cDSP results with a final FEA. For instance, after selecting a design result for the foam liner or composite shell (in Section 2.3), we built and submitted a final FEA to compare to the cDSP result. This is a simple form of verification, and some would argue this is more of an interpolation. It would be better if we could build the final design and compare to the cDSP and a FEA result. However, because we are designing an isolated region of the helmet there is not meaningful way to build and test the resulting design. In the future, when we can design the entire helmet assembly, we will be able to verify our design with manufacturing and testing according to the NOCSAE standard test methods. In the next section, we discuss the next steps of our future work.

3.2 Future Work

There are several areas for improvement, listed in the previous section, that our group is interested in pursuing to continue to refine this method for multi-component product design. First, we plan to reformulate the current problem with respect to Robust design, then we plan to expand and refine the method until we can design quality, robust helmets, using specific player requirements to protect their brain.

3.2.1 Robust Helmet Design

Robust design method for improving the quality of a product or system by reducing the effects of uncertainty, without directly attempting to eliminate the sources. The robust design method was originally developed by Genichi Taguchi [75] in 1980.

Taguchi introduced the use of signal-to-noise ratios, orthogonal arrays, linear graphs, and accumulation analysis for generating information about the system early in the design stages to save time and money resulting from poor quality products in the manufacturing stage. With any product or process being designed, there are parameters that are controllable (control parameters) and uncontrollable (noise). Noise is a form of aleatory uncertainty that comes from a changing environment, product damage, or manufacturing imperfections. In design, both noise and control factors will influence the ability of a product/process to achieve a target. For manufacturing applications, his method was applicable to systems that needed to reduce noise and bring quality on target. He developed the signal-to-noise ratio (S/N) as a predictor of quality loss. In Taguchi robust design, a designer searches for the maximum S/N ratio. Only considering noise in the design of a product or process is a severe limitation and has been criticized by Chen et al. [76]. Further advances in robust design have addressed the S/N ratio as well as the variance of the system. We show a graphical relationship between a mean and target as well as the quality distribution (variance) and tolerance distribution in Figure 3.1 below.

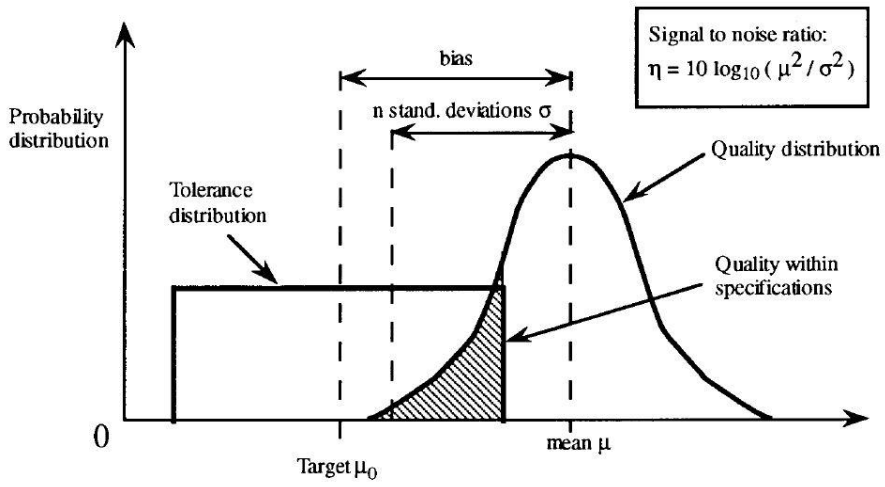

Figure 3.1 A signal-to-noise ratio used in robust design showing the relationship between the mean and target [65].

From a statistical standpoint, in robust design, a designer is concerned with two things: bringing the mean on target and minimizing the S/N ratio. To bring the mean on target, the system bias must be reduced. If the target is achieved but variation in quality is large, some products may fall outside the given tolerance range. By maximizing the S/N, the bell shape curve narrows and variation in quality is reduced. If the mean is on target and the S/N is high, there is a high probability your products will be within the given tolerance range.

Typically, in a robust design problem, there are three types of parameters: noise factors, control factors, and responses [77]. A noise factor is an uncontrollable parameter that affects the performance of a product or process. Noise factors are directly related to natural, aleatory uncertainty (NU). Control factors are parameters which a designer can control. As such, they are commonly referred to as “design variables.” There are several types of control factors and they are directly related to three common forms of epistemic uncertainty, namely, Model Parameter Uncertainty (MPU), Model Structural Uncertainty

(MSU), and Propagated Uncertainty (PU). A response is the measurable performance output of a system. In robust design problems, the noise factors, control factors, and responses are commonly represented by a P-diagram [78]. We show the generic form of a P-diagram in Figure 3.2 below.

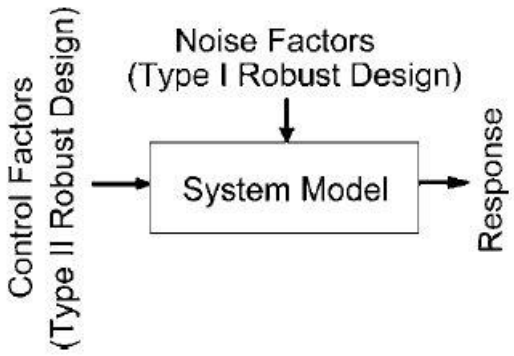

Figure 3.2 The generic P-Diagram used in robust design to represent system control factors, noise factors, and responses.

In Figure 3.2 above, we see the control factors and noise factors are fed into our system analysis and the responses are simply the system output. In our case, the noise factors and control factors would be listed in the "Given" section of the cDSP. In Figure 3.2, we refer to noise factors as "Type I Robust Design" and the control factors as "Type II Robust Design". There are actually four types of robust design:

- **Type I Robust Design [75]** – identify control factor (design variables) values that satisfy a set of performance requirement targets despite variation in **noise factors**.
- **Type II Robust Design [76]** – identify control factor (design variable) values that satisfy a set of performance requirement targets despite variation in **control and noise factors**.

- **Type III Robust Design [77]** – Identify adjustable ranges for control factors (design variable), that satisfy a set of performance requirement targets and/or performance requirement ranges and are insensitive to the variability **within the model**.
- **Type IV Robust Design [77]** – Identify adjustable ranges of control factors (design variables) values under potential uncertainty and **uncertainty propagation** in a design and analysis process chain; account for uncertainty in downstream activities and uncertainty propagation.

Taguchi [75] proposed Type 1 robust design to handle the variation problems associated with noise factors. Noise factors are usually given as environmental factors, operating conditions, boundary conditions, or material property variances. Variation for each of these is considered irreducible but can be measured statistically. Wei Chen et al. [76] proposed the use of Type II robust design when dealing with control factors. Control factors in the system model usually relate to system performance. Some examples of control factors are geometric parameters, mass, electrical, mechanical, or chemical inputs, amounts of constituents in materials, process control inputs, etc. [77]. An example of Type I and II robust design is shown below in Figure 3.3.

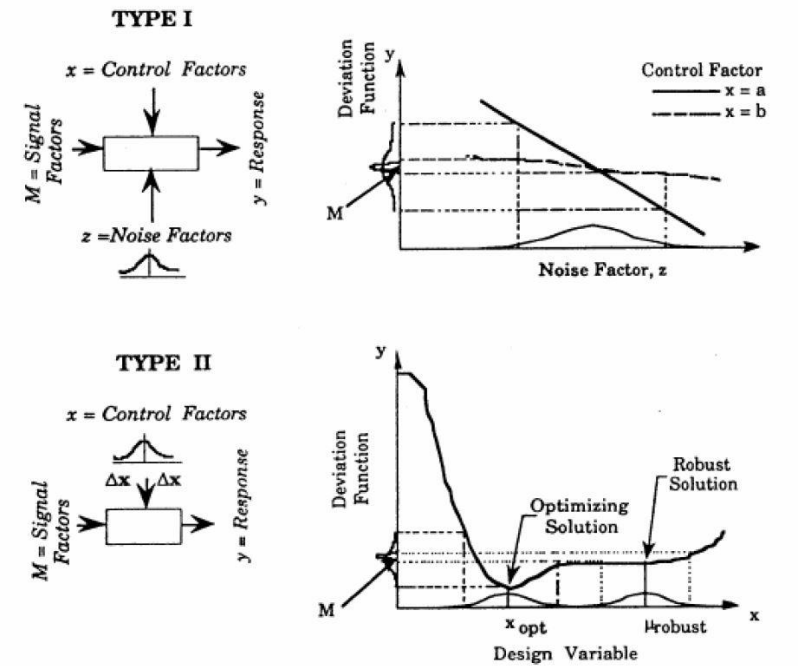

Figure 3.3 Robust design for variations in noise factors (Type I) and control factors (Type II) proposed by Chen et al. [76].

Chen's [76] P-Diagrams for Type I and Type II robust design are shown on the left half of Figure 3.3. The right half presents a schematic of the different concepts where Taguchi's [75] Type I is shown in the upper left. Taguchi's Type I robust design lets the designer choose between a set of control factor parameters so as to achieve the best S/N. In the schematic representation, control factor choices x = a, and x = b are presented. Option (a) represents a configuration that has a large amount of response variation with the variations of noise factors. However, with choice (b), the system response has very little variation. Assuming the mean is on target and the noise factors themselves cannot be reduced, the designer should select option b. Type I robust design only works if the mean of the system response is already on target. Type II robust design allows the designer to alter control factors so as to first bring the mean on target. Then the designer can select a design which also has low system response variation. The schematic in the

bottom left of Figure 3.3 represents a Type II robust design. Type II robust design is considered a dynamic problem where the response is a function of input parameters. As such, the curve in this figure represents a system response curve where changes in the design variable are along the x-axis and changes in system response are along the y-axis. Here, it is noted that the optimal design is found in the valley. However, at the optimal location, the variation in the system results in a large variation in system response. The designer should instead search for a location which has a mean on target and also demonstrates low response variation. This location is found at the plateau region and is the robust design. Both Type I and II robust design approaches are good for determining a set of parameters for a product or process that needs to be robust against real world variability. However, they both assume your analysis models are complete and accurate. Choi et al. [77] proposed Type III robust design to address the uncertainty in math or analysis models (MSU). Choi et al. [77] identifies the different forms of MSU come from linearization and discretization errors in FEA models, errors in computer codes, employment of uncertain knowledge, and other assumptions made from limited information. An example of Type III robust design is shown below in Figure 3.4.

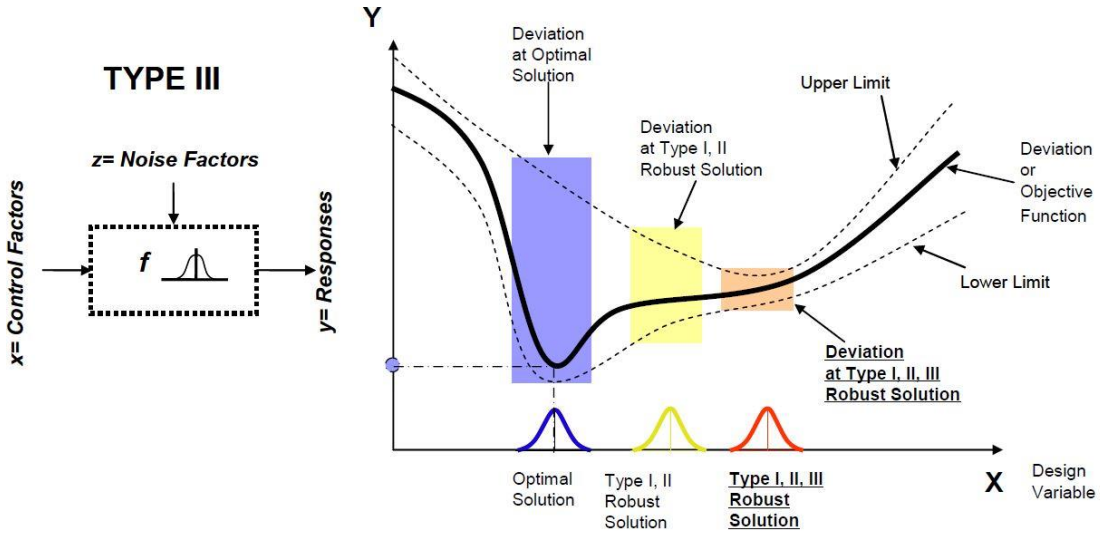

Figure 3.4 An example objective function showing the variability in the optimal solution versus Type I, II, and III robust solutions [77].

In Figure 3.4, the solid black line is the same objective function used by Chen et al. [76] in Figure 3.3. The two dashed lines above and below the objective function represent uncertainty limits. Bounding boxes are useful for visualizing the variation in response between design methods. If a designer were to assume their models were complete and accurate, then they would select the optimal design found in the valley of the response curve. It is clear to see that when natural uncertainty (NU) and model structural uncertainty (MSU) are introduced, that optimal design can actually have the greatest variation in system response. In this particular problem, a response that large is bound to fall outside the acceptable range, which could be catastrophic. Even the type I/II robust design selected previously now has a larger system variation and is not the best solution. The orang box is clearly the best as it provides a design choice with the smallest system response variation. This decision can only be made by compounding Type I, II, and III robust design. Due to the highly non-linear problems faced by engineering designers it is important that efforts

be made to quantify MSU and implement Type III robust design. The final Type IV robust design corresponds to the uncertainty that may propagate through complex design processes involving multiple disciplines or analysis chains comes from: (a) changes in design specifications from downstream design activity, or (b) propagation and amplification of uncertainty from parallel or series analysis tasks [77]. Consider Olson's [79] materials design paradigm example shown below in Figure 3.5.

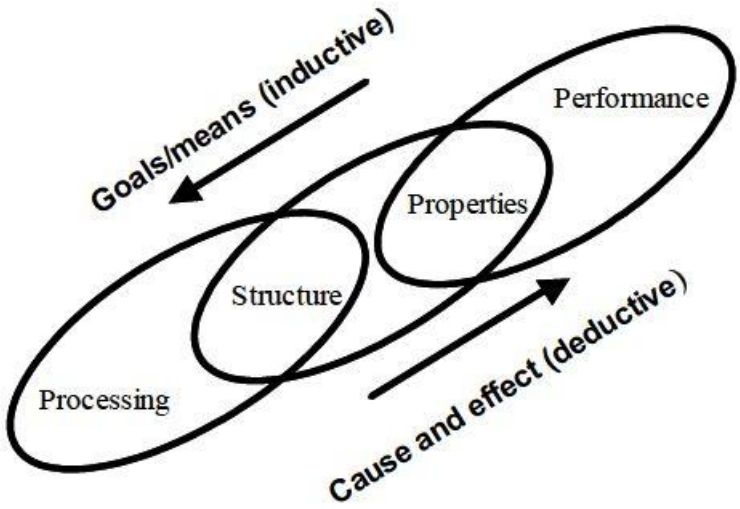

Figure 3.5 Olson's [79] material design bottom-up and top-down analysis chain.

Olson's [79] material design bottom-up and top-down analysis chain in Figure 3.5 above represents the linkage and overlap from a material processing, structure, property and performance. A designer either begins at the ground level with processing specifications, or at the top level with performance specifications and works their way through the chain. Often times, teams of scientists, engineers, and designers are working on the same design chain simultaneously. In complex models like Figure 3.5 analysis outputs can be passed to other inputs hierarchically, in parallel, or in series. Complex

design problems like these have high potential for propagating and amplifying uncertainty at any point in the design stage.

We can incorporate Type I, II, and III robust design into our current goal-oriented, inverse decision-based design method with specific robust goals, where the design analysis is still supported by the CEF and the cDSP. However, Nellippallil et al. [73] proposes using two new metrics for Type I, II, and III with Design Capability Indices (DCIs) for Type I and II, and Error Margin Indices (EMIs) for Type III. Essentially the DCIs and EMIs are formulated in the cDSP where the DCIs correspond to solutions that are robust against NU and MPU and the EMIs correspond to MSU. The resulting "robust satisficing solutions" are solutions whose mean and variation satisfy the conflicting goals and constraints. With respect to helmet design, we would formulate DCIs for every design variable from NU and MPU information, and EMIs for every polynomial response model from MSU information. More information regarding the DCIs and EMIs formulation can be found in [54].

3.2.2 Future Design Method Expansion and Refinement

In this thesis, we exercised the goal-oriented, inverse decision-based design framework to lay the foundation for helmet design. We were able to first map design requirements between two components with respect to a common set of system-level goals. Then, we found designs for both components in an inverse fashion with respect to these goals. While we demonstrate the method to design two components, this work was foundational for future helmet design where we will expand the current formulation to model and design the entire helmet system.

To accomplish the complete helmet design, we will first update the current method to include the bio-inspired inner shell with sutures and the stress wave dampers. We believe both components may play an important role in dissipating the stress waves, thus helping the system achieve the impulse goal (goal 3). Next, we will include the full-scale components including Velcro and TPU film for the foam liner, paint on the composite shell, etc. Then we will reformulate the system input and desired output using real player specific information. After we are satisfied with the results from the helmet region, we will expand the problem to a full-scale helmet where we can make simple modifications to design the other helmet regions including the brain's response as a performance goal. In the full-scale analysis, we believe the individual helmet regions could be modeled as the individual components were here in this thesis, and for each analysis, we would design the individual components with respect to the region goals. Once we have a fully functioning, full-scale design problem that describes the individual regions, and their associated components, with respect to the brain's performance, we can then tailor the design problem to design helmets for individual football players. Upon request, we could generate a helmet design specific for a player's head shape, age, brain injury history, and position. Finally, we believe our framework is general enough that we could repeat this process to design helmets for other sports such as hockey, lacrosse, or baseball.

REFERENCES

[1]. Shannon-Missal, Larry. “Pro Football is Still America’s Favorite Sport.” The Harris Poll. https://theharrispoll.com/new-york-n-y-this-is-a-conflicting-time-for-football-fans-on-the-one-hand-with-the-big-game-50-no-less-fast-approaching-its-a-time-of-excitement-especial/ (retrieved February 19, 2019).

[2]. “The History of Riddell.” Riddell. http://www.riddell.com/history/ (retrieved February 19, 2019).

[3]. Gurdjian, E. S., John E. Webster, and Herbert R. Lissner. "Studies on skull fracture with particular reference to engineering factors." The American Journal of Surgery 78, no. 5 (1949): 736-742.

[4]. Lissner, H. R., M. Lebow, and F. G. Evans. "Experimental studies on the relation between acceleration and intracranial pressure changes in man." Surgery, gynecology & obstetrics 111 (1960): 329.

[5]. Patrick, Lawrence M., Herbert R. Lissner, and Elisha S. Gurdjian. "Survival by design: Head protection." In Proceedings: American Association for Automotive Medicine Annual Conference, vol. 7, pp. 483-499. Association for the Advancement of Automotive Medicine, 1963.

[6]. Kucera, K. L., D. Klossner, B. Colgate, and R. C. Cantu. "Annual survey of football injury research: 1931–2015." National Center for Catastrophic Sport Injury Research Web site. https://nccsir. unc. edu/files/2013/10/Annual-Football-2015-Fatalities-FINAL. pdf. Accessed January 16 (2017).

[7]. Gadd, C.W., Use of a weighted-impulse criterion for estimating injury hazard. SAE Technical Papers, 1966.

[8]. NOCSAE, Standard Performance Specification for Newly Maufactured Football Helmets. 2011. Paper No. 002-11m11a.

[9]. Versace, John. A review of the severity index. No. 710881. SAE Technical Paper, 1971.

[10]. E.S. Gurdjian, H.R. Lissner, F.R. Latimerr, B.F. Haddad, J.E. Webster, Quantitative determination of acceleration and intercranial pressure in experimental head injury, Neurology 3 (1953) 417~423.

[11]. E.S. Gurdjian, V.R. Hodgsom, W.G. Hardy, L.M. Patrick, H.R. Lissner, Evaluation of the protective characteristics of helmets in sports, J. Trauma 4 (1964) 273 286

[12]. E.S. Gurdjian, V.L. Roberts, L.M. Thomas, Tolerance curves of acceleration and intracranial pressure and protective index in experimental head injury, J. Trauma 6 (1966) 600 604

[13]. Hutchinson, John, Mark J. Kaiser, and Hamid M. Lankarani. "The head injury criterion (HIC) functional." Applied mathematics and computation 96, no. 1 (1998): 1-16.

[14]. Prasad, Priya, and Harold J. Mertz. "The position of the United States delegation to the ISO Working Group 6 on the use of HIC in the automotive environment." SAE transactions (1985): 106-116.

[15]. Holbourn, A. H. S. "Mechanics of head injuries." The Lancet 242, no. 6267 (1943): 438-441.

[16]. Ommaya, Ayub K., Arthur E. Hirsch, and John L. Martinez. The role of whiplash in cerebral concussion. No. 660804. SAE Technical Paper, 1966.

[17]. Ommaya, A. K., and A. E. Hirsch. "Tolerances for cerebral concussion from head impact and whiplash in primates." Journal of biomechanics 4, no. 1 (1971): 13-21.

[18]. Pellman, Elliot J., David C. Viano, Andrew M. Tucker, Ira R. Casson, and Joe F. Waeckerle. "Concussion in professional football: reconstruction of game impacts and injuries." Neurosurgery 53, no. 4 (2003): 799-814.

[19]. Pellman, Elliot J., David C. Viano, Andrew M. Tucker, and Ira R. Casson. "Concussion in professional football: Location and direction of helmet impacts—Part 2." Neurosurgery 53, no. 6 (2003): 1328-1341.

[20]. Zhang, Liying, King H. Yang, Ramesh Dwarampudi, Kiyoshi Omori, Tieliang Li, Kun Chang, Warren N. Hardy, Tom B. Khalil, and Albert I. King. Recent advances in brain injury research: a new human head model development and validation. No. 2001-22-0017. SAE Technical Paper, 2001.

[21]. Zhang, Liying, King H. Yang, and Albert I. King. "A proposed injury threshold for mild traumatic brain injury." Journal of biomechanical engineering 126, no. 2 (2004): 226-236.

[22]. Patton, Declan A., Andrew S. McIntosh, and Svein Kleiven. "The biomechanical determinants of concussion: finite element simulations to investigate brain tissue deformations during sporting impacts to the unprotected head." Journal of applied biomechanics 29, no. 6 (2013): 721-730.

[23]. Funk, James R., S. M. Duma, S. J. Manoogian, and S. Rowson. "Biomechanical risk estimates for mild traumatic brain injury." In Annual Proceedings/Association for the Advancement of Automotive Medicine, vol. 51, p. 343. Association for the Advancement of Automotive Medicine, 2007.

[24]. McCaffrey, Meghan A., Jason P. Mihalik, Dean H. Crowell, Edgar W. Shields, and Kevin M. Guskiewicz. "Measurement of head impacts in collegiate football players: clinical measures of concussion after high-and low-magnitude impacts." Neurosurgery 61, no. 6 (2007): 1236-1243.

[25]. Broglio, Steven P., Jacob J. Sosnoff, SungHoon Shin, Xuming He, Christopher Alcaraz, and Jerrad Zimmerman. "Head impacts during high school football: a biomechanical assessment." Journal of athletic training 44, no. 4 (2009): 342-349.

[26]. Broglio, Steven P., Brock Schnebel, Jacob J. Sosnoff, Sunghoon Shin, Xingdong Feng, Xuming He, and Jerrad Zimmerman. "The biomechanical properties of concussions in high school football." Medicine and science in sports and exercise 42, no. 11 (2010): 2064.

[27]. Duma, Stefan M., and Steven Rowson. "Every newton hertz: a macro to micro approach to investigating brain injury." In 2009 Annual International Conference of the IEEE Engineering in Medicine and Biology Society, pp. 1123-1126. IEEE, 2009.

[28]. Rowson, Steven, Gunnar Brolinson, Mike Goforth, Dave Dietter, and Stefan Duma. "Linear and angular head acceleration measurements in collegiate football." Journal of biomechanical engineering 131, no. 6 (2009): 061016.

[29]. Rowson, Steven, Stefan M. Duma, Jonathan G. Beckwith, Jeffrey J. Chu, Richard M. Greenwald, Joseph J. Crisco, P. Gunnar Brolinson, Ann-Christine Duhaime, Thomas W. McAllister, and Arthur C. Maerlender. "Rotational head kinematics in football impacts: an injury risk function for concussion." Annals of biomedical engineering 40, no. 1 (2012): 1-13.

[30]. Duhaime, Ann-Christine, Jonathan G. Beckwith, Arthur C. Maerlender, Thomas W. McAllister, Joseph J. Crisco, Stefan M. Duma, P. Gunnar Brolinson et al. "Spectrum of acute clinical characteristics of diagnosed concussions in college athletes wearing instrumented helmets." Journal of neurosurgery 117, no. 6 (2012): 1092-1099.

[31]. Crisco, Joseph J., Bethany J. Wilcox, Jason T. Machan, Thomas W. McAllister, Ann-Christine Duhaime, Stefan M. Duma, Steven Rowson, Jonathan G. Beckwith, Jeffrey J. Chu, and Richard M. Greenwald. "Magnitude of head impact exposures in individual collegiate football players." Journal of applied biomechanics 28, no. 2 (2012): 174-183.

[32]. Rowson, Steven, and Stefan M. Duma. "Brain injury prediction: assessing the combined probability of concussion using linear and rotational head acceleration." Annals of biomedical engineering 41, no. 5 (2013): 873-882.

[33]. Rowson, Steven, Stefan M. Duma, Richard M. Greenwald, Jonathan G. Beckwith, Jeffrey J. Chu, Kevin M. Guskiewicz, Jason P. Mihalik et al. "Can helmet design reduce the risk of concussion in football?." Journal of neurosurgery 120, no. 4 (2014): 919-922.

[34]. Omalu, Bennet I., Steven T. DeKosky, Ryan L. Minster, M. Ilyas Kamboh, Ronald L. Hamilton, and Cyril H. Wecht. "Chronic traumatic encephalopathy in a National Football League player." Neurosurgery 57, no. 1 (2005): 128-134.

[35]. Baugh, Christine M., Julie M. Stamm, David O. Riley, Brandon E. Gavett, Martha E. Shenton, Alexander Lin, Christopher J. Nowinski, Robert C. Cantu, Ann C. McKee, and Robert A. Stern. "Chronic traumatic encephalopathy: neurodegeneration following repetitive concussive and subconcussive brain trauma." Brain imaging and behavior 6, no. 2 (2012): 244-254.

[36]. Mez, Jesse, Daniel H. Daneshvar, Patrick T. Kiernan, Bobak Abdolmohammadi, Victor E. Alvarez, Bertrand R. Huber, Michael L. Alosco et al. "Clinicopathological evaluation of chronic traumatic encephalopathy in players of American football." Jama 318, no. 4 (2017): 360-370.

[37]. Boston University Research: CTE Center. “Frequently Asked Questions About CTE.” Boston University Research: CTE Center. http://www.bu.edu/cte/about/frequently-asked-questions/ (retrieved February 19, 2019).

[38]. Ann C. McKee, Thor D. Stein, Christopher J. Nowinski, Robert A. Stern, Daniel H. Daneshvar, Victor E. Alvarez, Hyo-Soon Lee, Garth Hall, Sydney M. Wojtowicz, Christine M. Baugh, David O. Riley, Caroline A. Kubilus, Kerry A. Cormier, Matthew A. Jacobs, Brett R. Martin, Carmela R. Abraham, Tsuneya Ikezu, Robert Ross Reichard, Benjamin L. Wolozin, Andrew E. Budson, Lee E. Goldstein, Neil W. Kowall, Robert C. Cantu, The spectrum of disease in chronic traumatic encephalopathy, Brain, Volume 136, Issue 1, January 2013, Pages 43–64, https://doi.org/10.1093/brain/aws307

[39]. The Associated Press. “NFL, ex-players agree to $765M Settlement in Concusions Suit.” NFL. http://www.nfl.com/news/story/0ap1000000235494/article/nfl-explayers-agree-to-765m-settlement-in-concussions-suit (retrieved February 19, 2019).

[40]. NFL Enterprises LLC. “About Play Smart. Play Safe. And the NFL’s Health and Safety Commitment.” NFL. https://www.playsmartplaysafe.com/about/ (retrieved February 19, 2019).

[41]. Johnson, K. L., S. Chowdhury, W. B. Lawrimore, Y. Mao, A. Mehmani, R. Prabhu, G. A. Rush, and M. F. Horstemeyer. "Constrained topological optimization of a football helmet facemask based on brain response." Materials & Design 111 (2016): 108-118.

[42]. Viano D.C. (2005) Head Impact Biomechanics in Sport. In: Gilchrist M.D. (eds) IUTAM Symposium on Impact Biomechanics: From Fundamental Insights to Applications. Solid Mechanics and Its Applications, vol 124. Springer, Dordrecht

[43]. Craig, Matthew J. Biomechanics of jaw loading in football helmet impacts. Wayne State University, 2007.

[44]. Prabhu, Raj, Mark F. Horstemeyer, M. T. Tucker, E. B. Marin, Jean-Luc Bouvard, J. A. Sherburn, Jun Liao, and Lakiesha N. Williams. "Coupled experiment/finite element analysis on the mechanical response of porcine brain under high strain rates." Journal of the mechanical behavior of biomedical materials 4, no. 7 (2011): 1067-1080.

[45]. Francis, D. K., Jean-Luc Bouvard, Y. Hammi, and Mark F. Horstemeyer. "Formulation of a damage internal state variable model for amorphous glassy polymers." International Journal of Solids and Structures 51, no. 15-16 (2014): 2765-2776.

[46]. Nahum, Alan M., Randall Smith, and Carley C. Ward. Intracranial pressure dynamics during head impact. No. 770922. SAE Technical Paper, 1977.

[47]. Deb, Kalyanmoy. "A fast elitist non-dominated sorting genetic algorithm for multi-objective optimization: NSGA-2." IEEE Trans. Evol. Comput. 6, no. 2 (2002): 182-197.

[48]. Rush, Gustavus Alston. "Design of an American Football Helmet Liner for Concussion Mitigation." Order No. 10141627, Mississippi State University, 2016. https://login.proxy.library.msstate.edu/login?url=https://search.proquest.com/docview/1822268770?accountid=34815.

[49]. Trim, Michael Wesley. "Structure Property Relations and Finite Element Analysis of Ram Horns: A Pathway to Energy Absorbent Bio-Inspired Designs." Order No. 3466590, Mississippi State University, 2011. https://login.proxy.library.msstate.edu/login?url=https://search.proquest.com/docview/884789616?accountid=34815.

[50]. Johnson, Kyle Leslie. "From Horns to Helmets: Multi-Objective Design Optimization Considerations to Protect the Brain." Order No. 10141573, Mississippi State University, 2016. https://login.proxy.library.msstate.edu/login?url=https://search.proquest.com/docview/1822210867?accountid=34815.

[51]. Johnson, K. L., M. W. Trim, M. F. Horstemeyer, N. Lee, L. N. Williams, J. Liao, H. Rhee, and R. Prabhu. "Geometric effects on stress wave propagation." Journal of biomechanical engineering 136, no. 2 (2014): 021023.

[52]. Lee, Nayeon, M. F. Horstemeyer, R. Prabhu, Jun Liao, Hongjoo Rhee, Youssef Hammi, Robert D. Moser, and Lakiesha N. Williams. "The geometric effects of a woodpecker's hyoid apparatus for stress wave mitigation." Bioinspiration & biomimetics 11, no. 6 (2016): 066004.

[53]. Allen, J. K., Panchal, J. P., Mistree, F., Singh, A. K., and Gautham, B. P., 2015, "Uncertainty Management in the Integrated Realization of Materials and Components." In Proceedings of the 3rd World Congress on Integrated Computational Materials Engineering (ICME 2015), pp. 339–346.

[54]. McDowell, D. L., Panchal, J., Choi, H.-J., Seepersad, C., Allen, J. and Mistree, F., 2009, "Integrated Design of Multiscale, Multifunctional Materials and Products," Butterworth- Heinemann.

[55]. Nellippallil, A. B., Rangaraj, V., Gautham, B. P., Singh, A. K., Allen, J. K., and Mistree, F., 2018, "An Inverse, Decision-Based Design Method for Integrated Design Exploration of Materials, Products and Manufacturing Processes," Journal of Mechanical Design, vol. 140, no. 11, pp. 111403

[56]. Nellippallil, Anand Balu. "The Integrated Realization of Materials, Products and Associated Manufacturing Processes." (2018).

[57]. Gero, J. S., 1990, "Knowledge-Based Design Systems," Addison-Wesley

[58]. Suh, N. P., 1990, "The Principles of Design," Oxford University Press on Demand.

[59]. Mistree, F., Smith, W., Bras, B., Allen, J. and Muster, D., 1990, "Decision-Based Design: A Contemporary Paradigm for Ship Design," Transactions, Society of Naval Architects and Marine Engineers, vol. 98, no., pp. 565-597

[60]. Mistree, F., Smith, W., Kamal, S. and Bras, B., 1991, "Designing Decisions: Axioms, Models and Marine Applications," Fourth International Marine Systems Design Conference, pp. 1-24.

[61]. Mistree, F., Smith, W. and Bras, B., 1993, "A Decision-Based Approach to Concurrent Design," Concurrent Engineering, Springer, pp. 127-158.

[62]. Simon, H. A., 1969, "The Sciences of the Artificial," MIT Press, Cambridge, MA

[63]. Miller, J. G., 1978, "Living Systems Theory," Behavioral Sciences, New York: McGraw Hill

[64]. Muster, D. and Mistree, F., 1988, "The Decision-Support Problem Technique in Engineering Design," The International Journal of Applied Engineering Education, vol. 4, no. 1, pp. 23-33.

[65]. Bras, B. and Mistree, F., 1993, "Robust Design using Compromise Decision Support Problems," Engineering Optimization, vol. 21, no. 3, pp. 213-239

[66]. Mistree, F., Hughes, O. F. and Bras, B. A., 1993, "The Compromise Decision Support Problem and the Adaptive Linear Programming Algorithm," Structural Optimization: Status and Promise, (Kamat, M. P., Ed.), AIAA, Washington, DC, pp. 247-286

[67]. Nellippallil, A. B., Song, K. N., Goh, C.-H., Zagade, P., Gautham, B. P., Allen, J. K., & Mistree, F. (2017). A Goal-Oriented, Sequential, Inverse Design Method for the Horizontal Integration of a Multistage Hot Rod Rolling System. Journal of Mechanical Design. https://doi.org/10.1115/1.4035555

[68]. Chen, W., Allen, J. K. and Mistree, F., 1997, "A Robust Concept Exploration Method for Enhancing Productivity in Concurrent Systems Design," Concurrent Engineering, vol. 5, no. 3, pp. 203-217

[69]. Wang, Ru, Anand Balu Nellippallil, Guoxin Wang, Yan Yan, Janet K. Allen, and Farrokh Mistree. "Systematic design space exploration using a template-based ontological method." Advanced Engineering Informatics 36 (2018): 163-177.

[70]. Nellippallil, Anand Balu, Kevin N. Song, Chung-Hyun Goh, Pramod Zagade, B. P. Gautham, Janet K. Allen, and Farrokh Mistree. "A goal oriented, sequential process design of a multi-stage hot rod rolling system." In ASME 2016 International Design Engineering Technical Conferences and Computers and Information in Engineering Conference, pp. V02BT03A007-V02BT03A007. American Society of Mechanical Engineers, 2016.

[71]. Nellippallil, Anand Balu, Vignesh Rangaraj, Janet K. Allen, Farrokh Mistree, B. P. Gautham, and Amarendra K. Singh. "A decision-based design method to explore the solution space for microstructure after cooling stage to realize the end mechanical properties of hot rolled product." In Proceedings of the 4th World Congress on Integrated Computational Materials Engineering (ICME 2017), pp. 353-363. Springer, Cham, 2017.

[72]. Nellippallil, Anand Balu, Vignesh Rangaraj, B. P. Gautham, Amarendra Kumar Singh, Janet K. Allen, and Farrokh Mistree. "A Goal-Oriented, Inverse Decision-Based Design Method to Achieve the Vertical and Horizontal Integration of Models in a Hot Rod Rolling Process Chain." In ASME 2017 International Design Engineering Technical Conferences and Computers and Information in Engineering Conference, pp. V02BT03A003-V02BT03A003. American Society of Mechanical Engineers, 2017.

[73]. Nellippallil, Anand Balu, Pranav Mohan, Janet K. Allen, and Farrokh Mistree. "Robust Concept Exploration of Materials, Products and Associated Manufacturing Processes." In ASME 2018 International Design Engineering Technical Conferences and Computers and Information in Engineering Conference, pp. V02BT03A010-V02BT03A010. American Society of Mechanical Engineers, 2018.

[74]. Zhou, Jie. "Experimental and numerical investigation of soft impact loading on aircraft materials." (2017).

[75]. Tsui, K-L., (1992) Overview of Taguchi Method and Newly Developed Statistical Methods for Robust Design. IIE Vol. 24. No. 5

[76]. Chen, Wei, Janet K. Allen, Kwok-Leung Tsui, and Farrokh Mistree. "A procedure for robust design: minimizing variations caused by noise factors and control factors." Journal of mechanical design 118, no. 4 (1996): 478-485.

[77]. Choi, Hae-Jin. "A robust design method for model and propagated uncertainty." PhD diss., Georgia Institute of Technology, 2005.

[78]. Allen, Janet K., Carolyn Seepersad, HaeJin Choi, and Farrokh Mistree. "Robust design for multiscale and multidisciplinary applications." Journal of Mechanical Design 128, no. 4 (2006): 832-843.

[79]. Olson, Gregory B. "Computational design of hierarchically structured materials." Science 277, no. 5330 (1997): 1237-1242.